bioRxiv preprint doi: https://doi.org/10.1101/2020.06.09.142927; this version posted October 10, 2020. The copyright holder for this preprint (which was not certified by peer review) is the author/funder, who has granted bioRxiv a license to display the preprint in perpetuity. It is made available under a CC-BY-NC-ND 4.0 International license.
Manuscript submitted to *Cell*

# Digital twinning of Cellular Capsule Technology: emerging outcomes from the perspective of porous media mechanics

**Stéphane Urcun[1,2,3], Pierre-Yves Rohan[1], Wafa Skalli[1], Pierre Nassoy[4], Stéphane P.A. Bordas[2*], Giuseppe Sciumè[3*]**

***For correspondence:**
stephane.bordas@alum.northwestern.edu (SPAB);
giuseppe.sciume@u-bordeaux.fr (GS)

[1]Institut de Biomécanique Humaine Georges Charpak, Arts et Métiers ParisTech, 151 bd de l'Hôpital, 75013, Paris, France; [2]Institute for Computational Engineering Sciences, Department of Engineering Sciences, Faculté des Sciences, de la Technologie et de Médecine, Université du Luxembourg, Campus Kirchberg, 6, rue Coudenhove-Kalergi, L-1359, Luxembourg.; [3]Institut de Mécanique et d'Ingénierie (I2M), Univ. Bordeaux, CNRS, ENSAM, Bordeaux INP, 33400 Talence, France.; [4]Institut d'Optique Graduate School, CNRS UMR 5298, F-33400 Talence, France.

**Abstract** Spheroids encapsulated within alginate capsules are emerging as suitable *in vitro* tools to investigate the impact of mechanical forces on tumor growth since the internal tumor pressure can be retrieved from the deformation of the capsule. Here we focus in particular on the Cellular Capsule Technology (CCT).
We show that a modeling approach accounting for the triphasic nature of the spheroid (it consists of extracellular matrix, tumor cells and interstitial fluid) offers a new perspective of analysis revealing that the pressure retrieved experimentally is representative of the average stress state in the multiphase continuum, so it cannot be interpreted as a direct picture of the pressure sustained by the tumor cells.
A multiphase reactive poro-mechanical model is cross-validated and proposed here as a suitable digital twin of the CCT experiment. Parameter sensitivity analyses on the digital twin allows us to show that the main parameters determining the encapsulated growth configuration are different from those which drive growth in free condition, confirming that radically different phenomena are at play. Multiphase reactive poro-mechanics emerges here as an exceptional theoretical framework to deeply understand CCT experiments, to confirm their hypotheses or further improve their design.

## Introduction

As a tumor grows, it deforms surrounding living tissues, which causes strains and associated stresses. Mechano-biology focuses on these mechanical forces and their interplay with biological processes which has been extensively studied experimentally (***Helmlinger et al.*** (***1997***)). Within this context, current mathematical models of tumor growth are becoming more and more reliable, complement experiments and are useful tools for understanding, explaining and building upon these experimental findings ***Jain et al.*** (***2014***).

bioRxiv preprint doi: https://doi.org/10.1101/2020.06.09.142927; this version posted October 10, 2020. The copyright holder for this preprint (which was not certified by peer review) is the author/funder, who has granted bioRxiv a license to display the preprint in perpetuity. It is made available under a CC-BY-NC-ND 4.0 International license.


This article focuses on the Cellular Capsule Technology (CCT), an experimental protocol developed by some of us in ***Alessandri et al.*** (***2013***) where multi-cellular tumor spheroids (MCTS) are cultured within spherical porous alginate capsules. These last, after confluence (*i.e.* when the MCTS comes in contact with the inner wall), work as mechanosensors; indeed, from their deformation one can retrieve the stress state within the MCTS. The interaction pressure between the MCTS and the capsule, coming from the basic action-reaction principle, is a capital information since as envisioned in ***Alessandri et al.*** (***2013***) could enable prediction of stress-induced phenotype alterations to characterize cell invasiveness. To this aim it is essential to quantify the critical pressure which induces the phenotype switch. Notably, it is also relevant to quantify the characteristic time of this process since one can infer that a relatively high pressure sustained by cell during a relatively short time does not lead to phenotype modifications.

Using the measured interaction pressure as a direct discriminant to predict the occurrence of the phenotype switch is very attractive also due to the simplicity of the concept. However, mechanistic digital twinning of the CCT experiment reveals here that directly linking the interaction pressure and the phenotype switch could be a simplistic shortcut since behind the simplicity (in the good sense of the word) of the MCTS-capsule concept, there is a behavior which is not trivially explainable with basic physical concepts. Actually, the interaction pressure is a quite overall consequence encompassing several mechanisms at a lower level of description. The mechanics of porous media, on which is founded the proposed digital twin of the CCT experiment in this contribution, has emerged here as an excellent paradigm to model and possibly reveal these mechanisms offering a new perspective from which one can better interpret and exploit results of the CCT.

It is important to notice that the internal structure of the MCTS is heterogeneous so viewing or modeling the MCTS as a homogeneous continuum is not correct from the mechanical point of view. Hence, the MCTS is modeled here as a multiphase continuum consisting of tumor cells, interstitial fluid and an extracellular matrix which provides a certain stiffness to the multiphase continuum. A direct consequence of the multiphase modeling is that we observe that in the post-confluence phase while cells are compressed (positive pressure) the interstitial fluid pressure is negative. This fact has a rational explication. Actually, an intake of mass (and volume) is needed from the external medium since the MCTS-capsule system increases its size. Equally interesting is the role of the ECM scaffold which is submitted to the effective stress, in the sense of porous media mechanics, and not to the measured interaction pressure. Indeed, the pressure measured experimentally is representative of the total stress tensor (the Cauchy stress tensor), so it provides an averaged picture of the real situation where each phase of the system is submitted to its own stress state. Mathematical modeling enables retrieving of the stress of each phase from the Biot's effective stress principle and the adopted multiphase formulation (the model is founded on the rigorous framework provided by the Thermodynamically Constrained Averaging Theory of ***Gray and Miller*** (***2014***)).

To guarantee the scientific relevance of numerical results the reliability of the model is demonstrated adopting a crossing validation methodology. This has allowed a step-by-step customization of the mathematical model, obtaining a mechanistic formulation which remains predictive also when the experimental conditions of CCT experiment are modified. Systematic sensibility analyses have been helpful for the analysis and interpretation of results, allowing for quantification of the relative relevance of mechanisms underlying tumor growth phenomenology.

The effective digital twinning of the MCTS-capsule system and emerging biophysical outcomes from the perspective of multiphase porous media mechanics constitute together the novelty of this work. Differently from existing modeling approaches, which are often phenomenological and either so simplistic or so complex that their utility is very weak, the proposed modeling approach is mechanistic and contains the suitable degree of complexity to be representative such a kind of experiments.

bioRxiv preprint doi: https://doi.org/10.1101/2020.06.09.142927; this version posted October 10, 2020. The copyright holder for this preprint (which was not certified by peer review) is the author/funder, who has granted bioRxiv a license to display the preprint in perpetuity. It is made available under a CC-BY-NC-ND 4.0 International license.
Manuscript submitted to bioRxiv

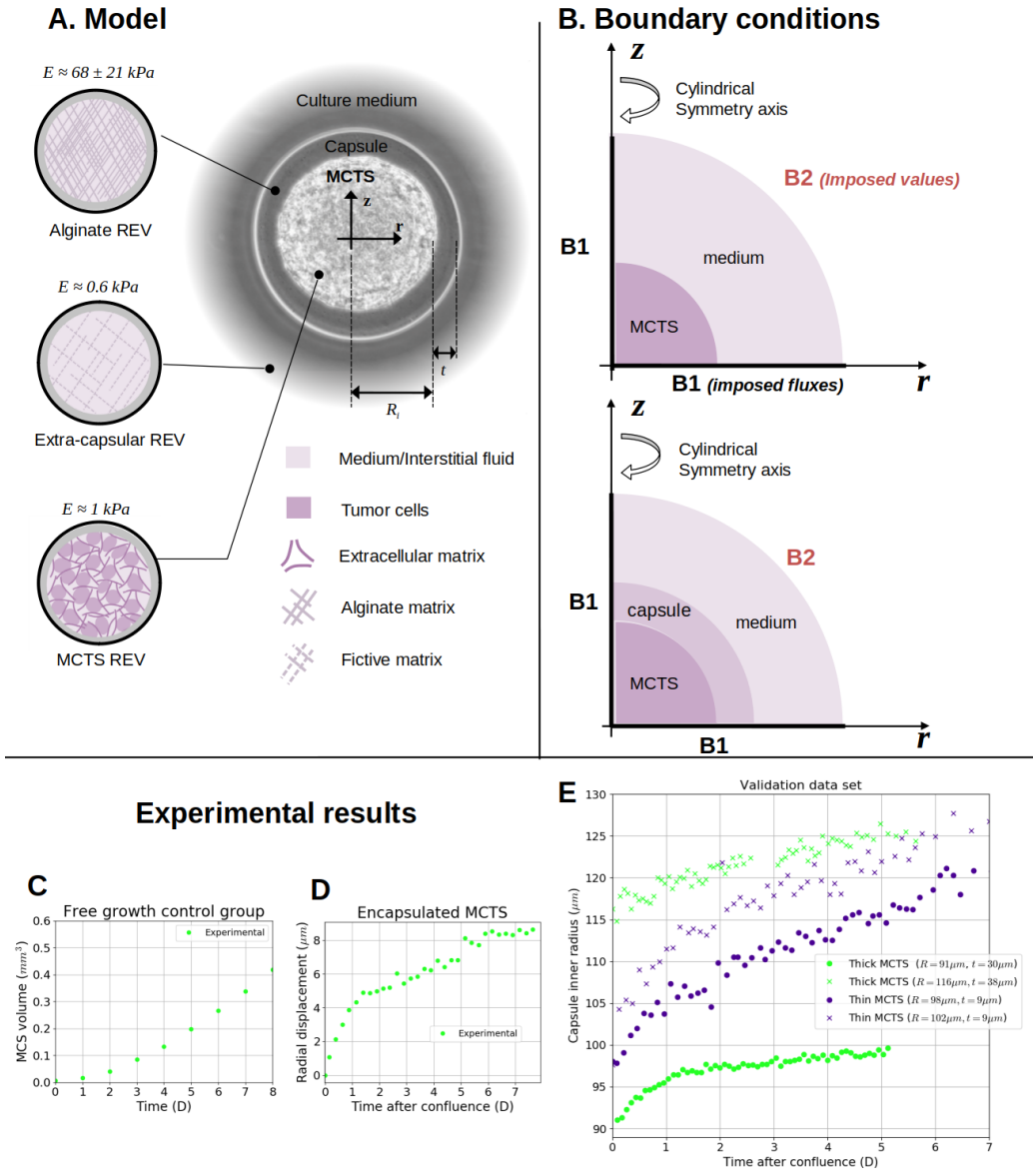





**Figure 1.** The capsule model. **A** Geometrical description of the capsule and assumed representative elementary volumes (REV): Three spatial domains modeled within the same mathematical framework: MCTS REV (consisting of tumor cells, interstitial fluid (IF) and extracellular matrix), the alginate shell (only IF phase within a solid scaffold of Young Modulus $E = 60$Kpa) and extra-capsular domain (only IF phase within a fictive solid scaffold of Young Modulus $E = 0.6$Kpa) enforced by the theoretical framework. **B** Computational boundary condition for the free (left) and confined (right) MCTS (see Methods and Model section, *In silico* reproduction process subsection). **C**-**E** Experimental input data. **C** Free MCTS control group, the volume is monitored over a time span of 8 days. **D** Encapsulated MCTS, the strain of a capsule (inner radius $R = 100\mu$m and thickness $t = 34\mu$m) is monitored a time span of 8 days. **E** Validation data set: two capsules, denoted as thick ($R = 91\mu$m, $t = 30\mu$m) and ($R = 116\mu$m, $t = 38\mu$m); two capsules, denoted as thin ($R = 98\mu$m, $t = 9\mu$m) and ($R = 102\mu$m, $t = 9\mu$m). Their strains are monitored over a time span of 5 to 7 days.

bioRxiv preprint doi: https://doi.org/10.1101/2020.06.09.142927; this version posted October 10, 2020. The copyright holder for this preprint (which was not certified by peer review) is the author/funder, who has granted bioRxiv a license to display the preprint in perpetuity. It is made available under a CC-BY-NC-ND 4.0 International license.


## Methods and Model

CCT offers an ideal framework to quantitatively assess the influence of mechanical stresses and its coupling with other biophysical factors impacting tumor cells proliferation and metabolism. Input data for the mathematical model can be retrieved from the CCT experimental conditions; furthermore, numerical results in term of pressure and displacement can be compared with those measured experimentally. This motivated the selection of CCT as reference experiment.

For the sake of clarity, the experimental observations reported by ***Alessandri et al.*** (***2013***)) together with some additional data provided by the authors are briefly recalled in subsection here-under. The mathematical model and the *in silico* reproduction process are then presented.

### Encapsulated MCTS: experimental procedure and observed phenomenology

MCTS cultures have been developed to overcome the constraints of 2D cultures, ***Cukierman et al.*** (***2001***), and investigate biophysical aspects (such as those involving integrine, the differentiation of epithelial cells, or the efficient deliver of a therapeutic agent) for which accounting the 3D nature of the tumor cell aggregate is essential.

MCTS can be cultured in free or confined conditions. ***Alessandri et al.*** (***2013***) recently proposed the CCT for developing confined MCTS cultures aiming at disclosing the interplay between the tumor and confinement mechanical forces which inhibit tumor growth ***Helmlinger et al.*** (***1997***), influence cell differentiation (mechanotransduction) and the acquisition of a cancerous phenotype ***Paszek et al.*** (***2005***). The developed method is based on the encapsulation and growth of cells inside permeable, elastic, hollow microspheres for the production of size-controlled MCTS. Alginate is used as a biomaterial for the encapsulation since its permeability permits the free flow of nutrients and oxygen and ensure favorable conditions for cellular growth without requiring additional molecules that could be potentially toxic for the MCTS.

Spherical alginate capsule with a diameter of a few hundreds of microns are built using a microfluidic co-extrusion device: the outer sheath is made of a sodium alginate solution; an intermediate compartment contains a calcium-free medium; and the inner core is composed of the cell suspension (CT26 mouse colon carcinoma). Performing extrusion in the air, the liquid jet is fragmented into droplets (due to Plateau-Rayleigh instability) which, upon contact with a calcium bath, readily crosslink as shells encapsulating cells (alginate undergoes gelation in the presence of divalent ions). The capsule allows convection of interstitial fluid and diffusion of nutrients species, growth factors and drugs through its surface; however, thanks to the alginate pores' size (of the order of 20 nm), cells cannot escape. The capsule therefore serves as micro-compartment for the 3D cell culture. During growth *in vivo*, the tumor deforms its surroundings which reacts with a confinement pressure. The mechanism is similar to what happens in the CCT experiment: during cell proliferation, the fraction of capsule volume occupied by cells increases until the capsule is filled (confluence); then the tumor spheroid starts to strongly interact with the capsule and deforms it. After confluence, the alginate capsule, deformed by the MCTS, responds with a confinement pressure due to action-reaction principle. This confinement pressure and non-optimal oxygenation of the MTCS core areas generate important measurable heterogeneities (necrosis, local increase in cell density, etc.) along the spheroid radius.

CCT allows generating capsules with desired size and shell thickness. This can be achieved by regulation of extrusion velocity and suitable geometrical adjustment of the co-extrusion device (see ***Alessandri et al.*** (***2013***) for more details). Before confluence, for all capsule thicknesses, the growth rate of the CT26 spheroid is almost the same as that of the free MCTS case, indicating that access to nutrients is not compromised by the presence of the alginate shell. After confluence, the behavior strongly deviates from that of the free MCTS case. Qualitatively, the same phenomenology is observed for all capsule thicknesses. However, results are quantitatively very different due to the different overall thickness of the alginate capsules.

The dilatation of the alginate capsule has been characterized as an elastic deformation with negligible plasticity and no hysteresis. Young's modulus was measured by atomic force microscopy

bioRxiv preprint doi: https://doi.org/10.1101/2020.06.09.142927; this version posted October 10, 2020. The copyright holder for this preprint (which was not certified by peer review) is the author/funder, who has granted bioRxiv a license to display the preprint in perpetuity. It is made available under a CC-BY-NC-ND 4.0 International license.
Manuscript submitted to *Cell*

indentation and osmotic swelling, giving a range of $68 \pm 21$kPa ***Alessandri et al.*** (***2013***). Thanks to the identified Young's modulus, capsules can be used as a biophysical dynamometer as a relation can be constructed which relates the variation of the inner pressure with radial deformation, monitored using video-microscopy.

### Experimental input data

Firstly, we considered the denoted training data set:

- for the free MCTS: the volume monitored over a time span of 8 days (***Figure 1***C);
- for the encapsulated MCTS: the strain of a capsule (inner radius $R = 100\mu$m and thickness $t = 34\mu$m) monitored for 8 days (***Figure 1***D);

The reliability of the mathematical model has been tested with the denoted validation data set (***Figure 1***E):

- Two capsules, denoted as thick ($R = 91\mu$m, $t = 30\mu$m) and ($R = 116\mu$m, $t = 38\mu$m);
- Two capsules, denoted as thin ($R = 98\mu$m, $t = 9\mu$m) and ($R = 102\mu$m, $t = 9\mu$m);

Sparse experimental data have been used to qualitatively measure the model emerging outcomes: the measurements of cell states (quiescent, proliferative, necrotic) of a small thick capsule ($R = 50\mu$m, $t = 12\mu$m), 26 hours after confluence, and the states of a $R = 50\mu$m free MCTS (see ***Figure 6***A, B).

## The mathematical model: a physics-based description of the MCTS-capsule system

Our understanding of the physics and mathematical modeling in oncology has made significant progress owing to our improved ability to measure physical quantities associated with the development and growth of cancer. Health research centers have been collaborating with engineers, mathematicians and physicists to introduce mechano-biology within clinical practice. This is particularly true for biochemical and genetic approaches which have been validated in patient cohorts, such as *e.g.* for the prediction of surgical volume for breast and prostate locations ***Edgerton et al.*** (***2011***), ***Lorenzo et al.*** (***2019***), and for the prediction of the chemical agent diffusion for pancreatic cancer ***Koay et al.*** (***2014***).

Three physics-based modeling approaches are currently used to model cancer: discrete, continuum and hybrid (the reader is referred to more detailed descriptions in the work of ***Lowengrub et al.*** (***2010***)). Among continuum models, poromechanical ones (*e.g.* see ***Sciumè et al.*** (***2013***); ***Mascheroni et al.*** (***2016***)) emerge today as valid approaches to model the interplay between biomechanical and biochemical phenomena. Following this promising trend, the multiphase reactive poro-mechanical model of ***Sciumè et al.*** (***2014a***) is here further developed and customized for digital twinning of CCT in order to reproduce numerically the experiment of ***Alessandri et al.*** (***2013***) gaining additional information not yet measurable *in vitro*.

Our approach considers the tumor tissue as a reactive porous multiphase system: tissue extracellular matrix constitutes the solid scaffold while interstitial fluid (IF) and tumor cells (TC) are modeled as fluid phases. Hence, the mathematical model is governed by momentum and mass conservation equations of phases and species constituting the MCTS-capsule system. Once the capsule is formed, three different spatial domains can be defined (***Figure 1***A): the intra-capsular domain where the tumor cells phase ($t$), the medium/interstitial fluid phase ($l$) and the extra-cellular matrix phase ($s$) coexist; the alginate shell domain, where a solid scaffold phase ($s$) and the medium fluid phase ($l$) coexist; and the extra-capsular domain where the only medium fluid phase ($l$) exist. In these three domains strains are calculated according to the theory of poro-elasticity which always assumes the presence of a certain solid phase volume fraction constituting the porous/fibrous medium. Therefore, a certain proportion of the solid phase must always be present even in the extra-capsular domain where it does not exist. Despite this unrealistic condition enforced by the

bioRxiv preprint doi: https://doi.org/10.1101/2020.06.09.142927; this version posted October 10, 2020. The copyright holder for this preprint (which was not certified by peer review) is the author/funder, who has granted bioRxiv a license to display the preprint in perpetuity. It is made available under a CC-BY-NC-ND 4.0 International license.


theoretical framework, the reliability of the model is only weakly affected, because the stiffness of this fictitious solid phase is two orders of magnitude lower than that of the alginate solid scaffold (***Figure 1***A). A unique physical model is defined for the three domains, with some penalty parameters (*e.g.* a low intrinsic permeability) avoiding cell infiltration in the alginate shell domain. Oxygen advection-diffusion within the medium/interstitial fluid phase is considered, oxygen acting as the limiting nutrient of TC, as prolonged hypoxia leading to the cell necrosis.
Starting from the general form of conservation equations provided by TCAT, the final system of governing equations is obtained. It consists of four equations:

- the $t$ phase mass conservation
- the $l$ phase mass conservation
- the advection-diffusion equation of oxygen in the $l$ phase
- the momentum conservation equation of the multiphase system

We have four primary variables: three are scalar and one vectorial.

- $p^l$ the pressure of the medium/interstitial fluid
- $p^{tl}$ the pressure difference between the cell phase $t$ and the medium/interstitial fluid $l$
- $\omega^{\tilde{n}l}$ the mass fraction of oxygen
- $\mathbf{u}^s$ the displacement of the solid scaffold

We also have two internal variables: the porosity $\varepsilon$ and the TC necrotic mass fraction $\omega^{Nt}$. The evolution of porosity is calculated from the mass conservation equation of the solid phase while the mass fraction of necrotic cells is updated according to the tissue oxygenation in the TC phase (see ***Sciumè et al.*** (***2013***)). We introduce two kinds of closure relationships for the system: mechanical and mechano-biological. Details about derivation of the governing equations and these constitutive relationships are provided in appendix Appendix A. The Multiphase System.

## Initial parameters settings

As prescribed in ***Brady and Enderling*** (***2019***), aiming biological or clinical relevancy demands to investigate each choice of the initial values of the parameters. Some parameters are of physical nature (the IF dynamic viscosity, the oxygen mass fraction inside cell cultures), they can be, even with difficulties, measured or at least their values will be compared to the physical soundness. Others parameters belongs more specifically to bio-poromechanical models in the mathematical oncology fields. Some of them have a quite theoretical nature (*e.g.* the 'permeability' of the ECM) while others have been experimentally measured at the cellular level (*e.g.* the oxygen consumption rate of EMT6/Ro cell line in ***Casciari et al.*** (***1992***)). For these parameters we have taken values that previous numerical studies (***Chignola et al.*** (***2000***), ***Sciumè et al.*** (***2014a***), ***Mascheroni et al.*** (***2016***), ***Santagiuliana et al.*** (***2019***)) have used for MCTS cultured with other cell lines (human glioblastoma multiforme and human malignant melanocytes), averaged these values, that we will denote '*generic*', and used them as initial guess for identification of parameters of our CT26 cell line based MCTS.
When experimental data did not provide any relevant information on a parameter (*e.g.* for ECM stiffness and permeability) and the sensitivity of the solution to their variation were insignificant ($< 1\%$ of the variance of the solution), we chose to fix them at their generic value.
The following parameters have a non negligible influence on the model outputs, and the closure relationships they belong are explained in detail in Appendix A. The Multiphase System:

- $\mu_t$ the TC dynamic viscosity (eq.19)
- $a$ the parameter tuning the joint impact of the ECM thinness and cell surface tension (eq.23)
- $\gamma_g^t$ the TC growth rate (eq.26)
- $\gamma_g^{nl}$ and $\gamma_0^{nl}$ the oxygen consumption rate due to growth and quiescent metabolism respectively (eq.29)

bioRxiv preprint doi: https://doi.org/10.1101/2020.06.09.142927; this version posted October 10, 2020. The copyright holder for this preprint (which was not certified by peer review) is the author/funder, who has granted bioRxiv a license to display the preprint in perpetuity. It is made available under a CC-BY-NC-ND 4.0 International license.


Two other parameters, $p_1$ and $p_{\text{crit}}$, are introduced in this modelling framework. They represent thresholds which govern the inhibition of the proliferation (eq.28) of cancer cells. The initial guess of $p_{\text{crit}}$ have been chosen according to the work of ***Helmlinger et al.*** (***1997***) and ***Paszek et al.*** (***2005***), and the value of $p_1$ has been set by observation of the experimental data.

## In-silico reproduction process

From the computational point of view, we aimed to a light and adaptable process: free, open source and compatible with any 2D or 3D geometry. For the model validation, we followed the convention of mathematical oncology proposed in ***Brady and Enderling*** (***2019***): two distinct sets of data for optimisation and validation, the parameters set being fixed before validation. To measure the quality of the fits, we followed the prescription of ***Benzekry et al.*** (***2014***): the root mean square error (RMSE) relatively to a reference, specified each time. The error on the numerical quantity $\xi_{\text{num}}$ relative to a reference $\xi_{\text{ex}}$, evaluated at $n$ points is:

$$RMSE(\xi_{\text{num}}, \xi_{\text{ex}}, n) = \sqrt{\frac{1}{n}\sum_{k=1}^{n}\left(\frac{\xi_{\text{ex}}(k) - \xi_{\text{num}}(k)}{\xi_{\text{ex}}(k)}\right)^2} \tag{1}$$

### Computational framework

We implemented the above model in Python and C++ within the FEniCS framework ***Alnæs et al.*** (***2015***), with an incremental monolithic resolution of the mixed finite element (FE) formulation. All the details and analytical verification of the FE formulation can be found in Appendix B. Computational framework.

The ***Figure 1***.B shows the two modeled configurations of MCTS (the free on the left and the confined on the right). Each mesh is a half of a sphere, because we also exploit symmetry with respect to a diametrical plane. For the three scalar variables, we prescribed Dirichlet boundary conditions along the outer radius of the domain $p^l = 0$, $p^{tl} = 0$, $\omega^{\bar{n}l} = 4.2e^{-6}$ [1] and no flux condition at $r = 0$ and $z = 0$. For the ECM displacement field $\mathbf{u}^s$, slip conditions $u_r^s = 0|_{r=0}$ and $u_z^s = 0|_{z=0}$ are used, and Dirichlet conditions $\mathbf{u}^s = \mathbf{0}$ at the outer radius of the domain (see ***Figure 1***.B).

### Sensitivity analysis, parameter identification and model validation

A global sensitivity analysis by Sobol indices was performed on the training data set to assess the sensitivity of the FE solution to the input parameters, both on the free and encapsulated MCTS.

- In the first order analysis, the 7 parameters ($mu_t$, $a$, $\gamma_g^t$, $\gamma_g^{nl}$, $\gamma_0^{nl}$, $p_1$, $p_{\text{crit}}$) were disturbed one at a time respectively to a $[-10, -5, -2, -1, +1, +2, +5, +10]\%$ grid. The variations of the solution were interpreted as a linear model, and the influence of a parameter $\alpha$ was deduced from the slope $\theta_\alpha$ of the linear fit. The Sobol index $S_\alpha$ was calculated as follows:

$$S_\alpha = \frac{\theta_\alpha^2}{\sum_i \theta_i^2} \tag{2}$$

- The 21 tuples were evaluated at the 2 extreme values of the grid for each configuration. The polynomial model allowed to compute two types of Sobol indices: $S_i$ for the influence of the parameter $i$ and $S_{ij}$ for the influence of each couple $(i, j)$ of parameters.

$$S_i = \frac{\theta_i^2}{\sum_i \theta_i^2 + \sum_{ij, i>j} \theta_{ij}^2} \quad \text{and} \quad S_{ij} = \frac{\theta_{ij}^2}{\sum_i \theta_i^2 + \sum_{ij, i>j} \theta_{ij}^2} \tag{3}$$

All the details of the process, auxiliary parameters and cost functions can be found in Appendix C. Sensitivity analysis.

For both configurations, the optimization procedure was based on sensitivity profiles, that is to say,

[1] which corresponds, according to Henry's law, to 90mmHg, the usual oxygen mass fraction in arteries (see ***Ortiz-Prado et al.*** (***2019***))

bioRxiv preprint doi: https://doi.org/10.1101/2020.06.09.142927; this version posted October 10, 2020. The copyright holder for this preprint (which was not certified by peer review) is the author/funder, who has granted bioRxiv a license to display the preprint in perpetuity. It is made available under a CC-BY-NC-ND 4.0 International license.


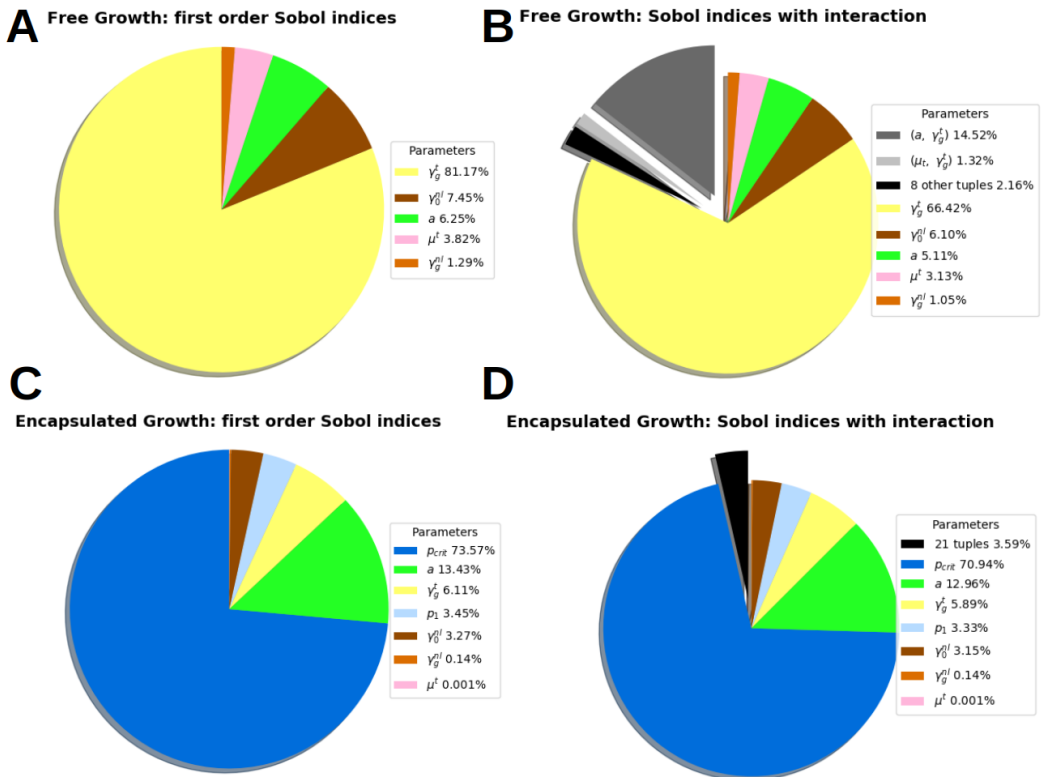


**Figure 2.** Sobol indices of the solution sensitivity on 7 parameters: $\mu_t$ the TC dynamic viscosity, the parameter $a$ accounting for the joint impact of the ECM thinness and cell surface tension, $\gamma_g^t$ the TC growth rate, $\gamma_g^{nl}$ and $\gamma_0^{nl}$ the oxygen consumption rate due to growth and quiescent metabolism respectively, $p_1$ and $p_{\text{crit}}$, two thresholds which govern the pressure-induced inhibition of the TC proliferation. Free MCTS configuration,**A**, First order analysis: Only 5 parameters remain, the governing parameter is $\gamma_g^t$, the tumor cells growth rate, the sensitivity of the solution on the pressure parameters, $p_1$ and $p_{\text{crit}}$, is 0. **B** Interaction: among 10 parameters tuples, one is significant $(a, \gamma_g^t)$ $14.5\%$ of the solution variance. Thus, these two parameters are not independent and should identified together. The total variance of the solution shows that, considering all the interactions, the influence of each parameter alone is not qualitatively changed: $\gamma_g^t$ from $81.1\%$ to $66.4\%$, $\gamma_0^{nl}$ from $7.4\%$ to $6.1\%$, $a$ from $6.2\%$ to $5.1\%$. Encapsulated MCTS configuration, **C**, First order analysis: the governing parameter is $p_{\text{crit}}$ the inhibitory pressure of tumor cells growth ($73.5\%$ of the solution variance). **D** Interaction: the sum of 21 parameters tuples represents $3.6\%$ of the solution variance (the detail of 21 tuples can be found in Appendix C. Sensitivity analysis, table 6).

we optimized the parameters that gathered $90\%$ of the variance of the solution. The selected parameters were identified by a Nelder-Mead simplex algorithm. In the encapsulated configuration, the parameters of the MCTS cell-line were identified in an alginate capsule with a stiffness of mean experimental value: $E = 68$ kPa. The optimized parameters set is shared by both configurations. To evaluate the reliability of the identified parameters, an author of this article and member of the team of ***Alessandri et al.*** (***2013***) have jointly provided unpublished experimental results of encapsulated MCTS, both thick and thin, namely the validation data set. As their alginate stiffness was not known (the Young's modulus of the alginate was estimated to be $E = 68 \pm 21$ kPa), two simulations were run for each capsule with the extreme values of $E$. This provided the range of modeling possibilities of the identified parameters.

## Results

Based on a detailed sensitivity study, the optimized set of parameters was tested and cross-validated on unpublished experimental results (***Figure 1***E) provided by the same team of ***Alessandri et al.*** (***2013***). Numerical simulation also provides a wide output of qualitative results which are presented

bioRxiv preprint doi: https://doi.org/10.1101/2020.06.09.142927; this version posted October 10, 2020. The copyright holder for this preprint (which was not certified by peer review) is the author/funder, who has granted bioRxiv a license to display the preprint in perpetuity. It is made available under a CC-BY-NC-ND 4.0 International license.


**Table 1.** Parameters for the CT26 cell line. Source of the generic values: ***Chignola et al.*** (***2000***), ***Sciumè et al.*** (***2014a***), ***Mascheroni et al.*** (***2016***), ***Santagiuliana et al.*** (***2019***)

| Parameter | Symb. | Generic | Unit | Optimized |
|---|---|---|---|---|
| ECM network thinness | $a$ | 800 | Pa | 890 |
| Dynamic viscosity of TC | $\mu_t$ | 36 | Pa.s | negligible |
| TC growth rate | $\gamma_g^t$ | $4.10^{-2}$ | kg/(m$^3$.s) | $3.33.10^{-2}$ |
| TC growth $O_2$ consump. | $\gamma_g^{nl}$ | $4.10^{-4}$ | kg/(m$^3$.s) | negligible |
| TC metabolism $O_2$ consump. | $\gamma_0^{nl}$ | $6.10^{-4}$ | kg/(m$^3$.s) | $6.65.10^{-4}$ |
| Start TC growth inhibitory | $p_1$ | 1800 | Pa | 1432 |
| Stop TC growth | $p_{\text{crit}}$ | 4000 | Pa | 5944 |

and interpreted. At the end of the section, we show that the model outputs allow to predict, with a reasonably good accuracy, experimental TC saturation and its necrotic fraction, despite these quantities have not been used for the model optimization.

## Sensitivity analysis

***Figure 2*** shows the results of first order and second-order interaction analyses, for the free and encapsulated configurations respectively. Clearly distinct profiles were obtained.

In the free MCTS configuration, the governing parameter is $\gamma_g^t$ the tumor cells growth rate (first order index, $S_{\gamma_g^t} = 81\%$, with interactions $S_{\gamma_g^t} = 66.4\%$). In decreasing order, we have two parameters that are not negligible: $\gamma_0^{nl}$ the oxygen consumption due to metabolism (first order index $7.45\%$, with interactions $6.10\%$) and $a$, the parameter determining the joint impact of the ECM thinness and cell surface tension (first order index $6.25\%$, with interactions $5.11\%$). The important difference between the 2 Sobol indices of $\gamma_g^t$ is explained by the only non negligible interaction between two parameters: $\gamma_g^t$ and $a$ ($S_{(a,\gamma_g^t)} = 14.5\%$, see ***Figure 2***, right). This important interaction is indicative of the significant roles that ECM properties and cell-cell adhesion have on proliferative-migration behavior (this is widely described in literature, see for instance ***Paszek et al.*** (***2005***)) and that our modeling approach can reproduce mechanistically how these properties impact the overall observed phenomenology of tumor growth. Thus, these two parameters are not independent and should be identified together.

For all parameters perturbations in the first order and second-order interaction analyses, the pressure of the TC phase $p^t = p^l + p^{tl}$ was less than $1$ KPa, thus the first threshold of growth inhibitory due to pressure $p_1$ was never reached and, *a fortiori*, the critical threshold of total inhibition $p_{\text{crit}}$. Thus, the sensitivity of the FE solution to $p_1$ and $p_{\text{crit}}$ was 0. The 3 parameters $\gamma_g^t$, $a$ and $\gamma_0^{nl}$ has therefore been optimized for the free configuration. For the encapsulated configuration, the governing parameter is the critical inhibitory pressure $p_{\text{crit}}$ (first order $S_{p_{\text{crit}}} = 73.5\%$, with interaction $70.9\%$). $\gamma_g^t$, $a$ and $\gamma_0^{nl}$ has already been identified for the free configuration, the only non negligible parameter remaining is $p_1$ (first order index $S_{p_1} = 3.4\%$, with interaction $3.3\%$). The difference between Sobol indices of first order and interactions is weak, indeed, the 21 parameters tuples gather only $3.6\%$ of the solution variance. Thus, in the encapsulated configuration the parameters can be considered non-correlated and be identified separately.

Such results allow us to highlight that in the encapsulated configuration the mechanical constraint is the phenomenon that determines the overall growth phenomenology provided by the mathematical model.

## Optimization

We identified the three governing parameters $\gamma_g^t, \gamma_0^{nl}, a$ for the free MCTS configuration by the Nelder-Mead simplex algorithm and fitted to the experimental data with a $RMSE = 0.031$. To be physically relevant, the same parameters set should be shared by the two configurations. Hence, these three

bioRxiv preprint doi: https://doi.org/10.1101/2020.06.09.142927; this version posted October 10, 2020. The copyright holder for this preprint (which was not certified by peer review) is the author/funder, who has granted bioRxiv a license to display the preprint in perpetuity. It is made available under a CC-BY-NC-ND 4.0 International license.
Manuscript submitted to bioRxiv

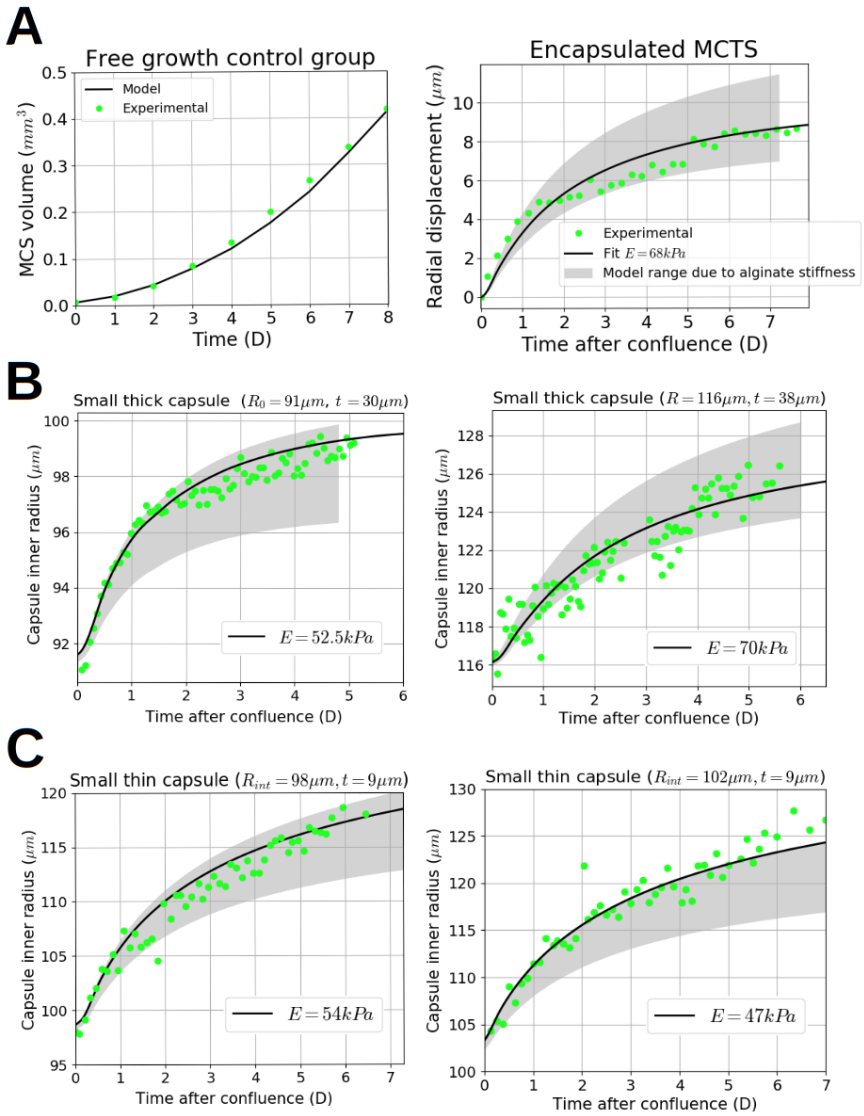


**Figure 3.** Validation of the optimized parameters. Alginate Young's was estimated in ***Alessandri et al.*** (***2013***) as $E = 68 \pm 21$ kPa. Simulations with the extreme values of $E$ give the range of possibilities of the optimized set predicted with the model. Experimental results, green dotted ; Numerical results with the optimized parameters set, black; Modeling range, grey filled. **A**. Left, free MCTS control group, Time (Day) versus MCTS volume (mm$^3$). Right, reference encapsulated MCTS (inner radius $100\mu$m, thickness $34\mu$m), time (Day) versus radial displacement ($\mu$m). Fit with $E = 68$kPa. **B** Validation of the identified parameters on 2 thick capsules. Time (Day) versus Capsule radius ($\mu$m). The experimental points are in the modeling range. Both capsule fit with $E = 52.5$kPa and $E = 70$kPa respectively. **C** Partial validation of the identified parameters on 2 thin capsules. Time (Day) versus Capsule radius ($\mu$m). Left, one capsule is fitted with $E = 54$kPa ; right, the experimental points are at the boundary of the modeling range.

bioRxiv preprint doi: https://doi.org/10.1101/2020.06.09.142927; this version posted October 10, 2020. The copyright holder for this preprint (which was not certified by peer review) is the author/funder, who has granted bioRxiv a license to display the preprint in perpetuity. It is made available under a CC-BY-NC-ND 4.0 International license.
Manuscript submitted to *Cell*

parameters were injected within the encapsulated configuration and its two governing parameters $p_1, p_{\text{crit}}$ were identified using the same algorithm. We fitted the experimental data of the encapsulation with a $RMSE = 0.124$. ***Figure 3***A shows the two configurations fitted with the following set of parameters: $\gamma_g^t = 3.33\,.10^{-2}$, $\gamma_0^{nl} = 6.65\,.10^{-4}$, $a = 890$, $p_1 = 1432$, $p_{\text{crit}} = 5944$ (see Table 1). This set is cell-line specific, only relevant for CT26 mouse colon carcinoma.

## Validation

Unpublished experimental results of encapsulated MCTS, both thick and thin, have been used as validation data set (***Figure 1***E). Each capsule had its own radius $R$ and thickness $t$ and two simulations have been run with the extreme experimental values of the alginate stiffness ($E = 47$kPa and $E = 89$kPa).

***Figure 3***A right shows the range of modeling possibilities of the identified parameters on the training data ($R = 100\mu$m, $t = 34\mu$m), respectively to the alginate stiffness range. The parameters set was identified with the mean stiffness value ($E = 68$kPa).

***Figure 3***B shows that the modeling range on two thick capsules is in accordance with the experimental results. Two fits with an alginate stiffness at $E = 52.5$kPa and $E = 70$kPa respectively are proposed.

The ***Figure 3***C shows results relative to two thin capsules. The dynamics is properly reproduced by the model for both capsules which are importantly deformed (the strain is of $16\%$ for the left one and $20\%$ for the right one). Despite in the right case (that with $R = 102\mu$m, $t = 9\mu$m) the model shows some limitations (note that the proposed fit is at the minimum stiffness value $E = 47$kPa) the presented cross-validation demonstrates that this mechanistic mathematical model can adapt to different geometries and thickness without losing its relevance. Focusing on the left graphs in figures B and C we can note that, with the same parameters set and almost the same alginate stiffness ($E_{B,\text{Left}} = 52.5$kPa and $E_{C,\text{Left}} = 54$kPa), the model reproduces experimental strain of $8\%$ and $16\%$ respectively. The difference between the two strains is induced by the geometrical effect due to the capsule thickness, which impacts on the evolution of internal stresses, cell growth and oxygen consumption.

## Qualitative results and emerging outcomes

In addition to overall quantitative results, ***Figure 4*** and ***Figure 5*** provide details on the physical phenomena occurring during growth (from confluence to 85 hours after confluence) of a MTCS encapsulated in a thick capsule with the same geometry used for identification of the input parameters of the mathematical model ($R = 100\mu$m, $t = 34\mu$m). These figures allow to quickly understand the importance of physics-based modeling, as it provides qualitative information that could be used to interpret the experimental process as a whole and to better understand the tumor growth process.

***Figure 4*** shows contours of oxygen, necrotic fraction, IF pressure, ECM displacement, TC pressure and TC saturation at confluence and 85 hours after. To gain information about the dynamics of these quantities, ***Figure 5*** shows them probed along the radius at confluence, 85 hours after, and at two intermediate times (28 and 56 hours).

***Figure 5***A and B show the interplay between oxygen consumption and necrosis. Indeed as mentioned in the experiments, 85 hours after confluence, the viable space remaining for TC is a $20\,\mu$m thick rim. This is explicit in ***Figure 4***, upper right circle, NTC quarter. The comparison of ***Figure 5***F and B shows a relation between the saturation of TC and their necrotic fraction. This is a basic experimental fact that, when the cells bodies collapse in a necrotic core, the aggregate density increases accordingly. ***Figure 5***D and E allow to 'visualize' the overall dynamics of the process: the capsule displacement strongly increases after confluence due to the contact with tumor cells whose pressure rises from 1.15 kPa at confluence to almost 4 kPa, 85h after confluence. Beyond 85h and until eight days after confluence, it was observed that the tumor cells pressure $p^t < p_{\text{crit}}$. This is in accordance with the experiment as recorded in ***Alessandri et al.*** (***2013***) where it was reported that the MCTS continued to grow twelve days after confluence, even very slowly. The tumor

bioRxiv preprint doi: https://doi.org/10.1101/2020.06.09.142927; this version posted October 10, 2020. The copyright holder for this preprint (which was not certified by peer review) is the author/funder, who has granted bioRxiv a license to display the preprint in perpetuity. It is made available under a CC-BY-NC-ND 4.0 International license.


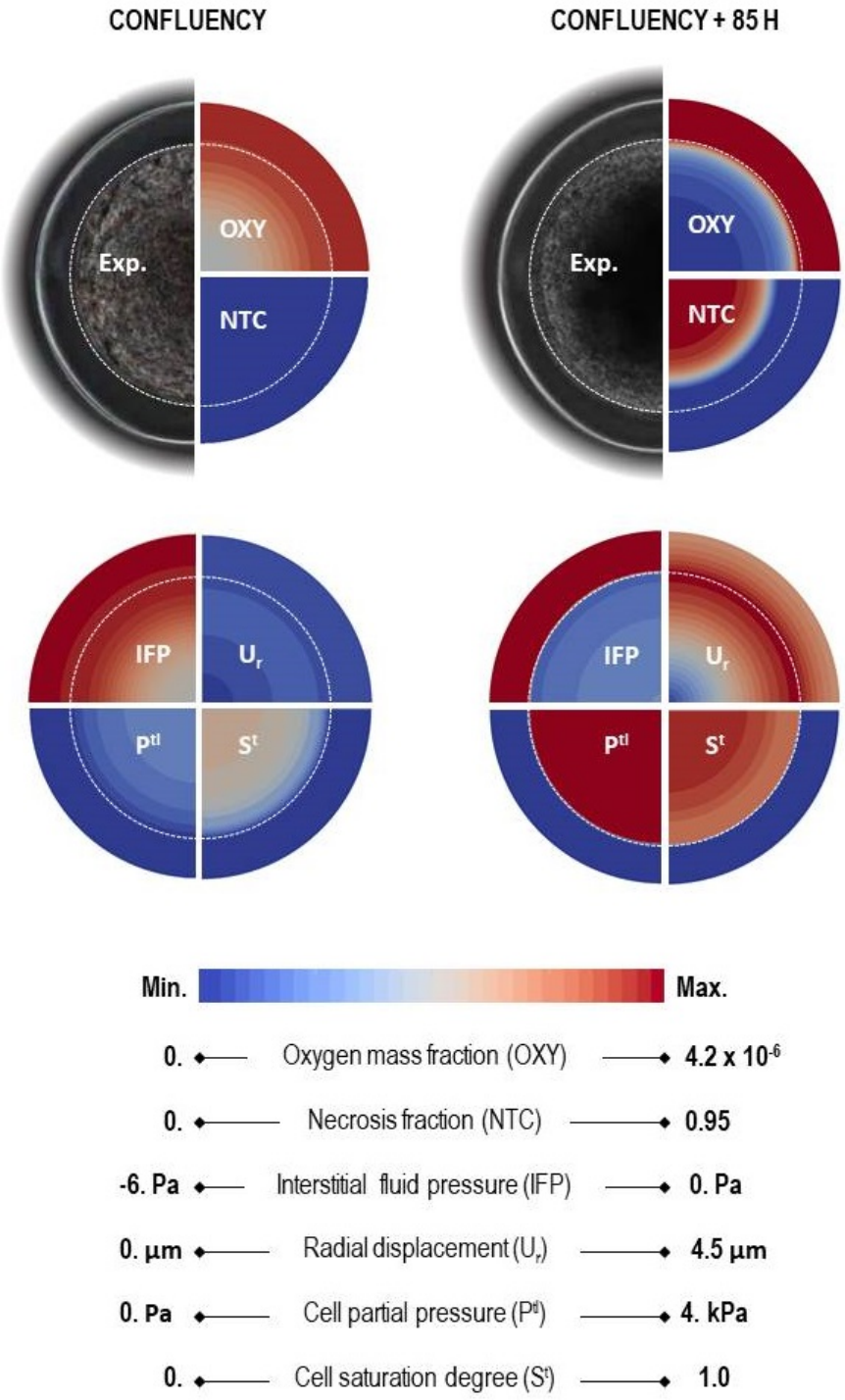


**Figure 4.** Experimental microscopy image augmented by 6 physical quantities from numerical results of the mathematical model: oxygen, necrotic tumor cells, interstitial fluid pressure, radial displacement, partial tumor cells pressure and tumor cells saturation. Left, at confluence. Right, 85 hours after confluence.

bioRxiv preprint doi: https://doi.org/10.1101/2020.06.09.142927; this version posted October 10, 2020. The copyright holder for this preprint (which was not certified by peer review) is the author/funder, who has granted bioRxiv a license to display the preprint in perpetuity. It is made available under a CC-BY-NC-ND 4.0 International license.
Manuscript submitted to bioRxiv

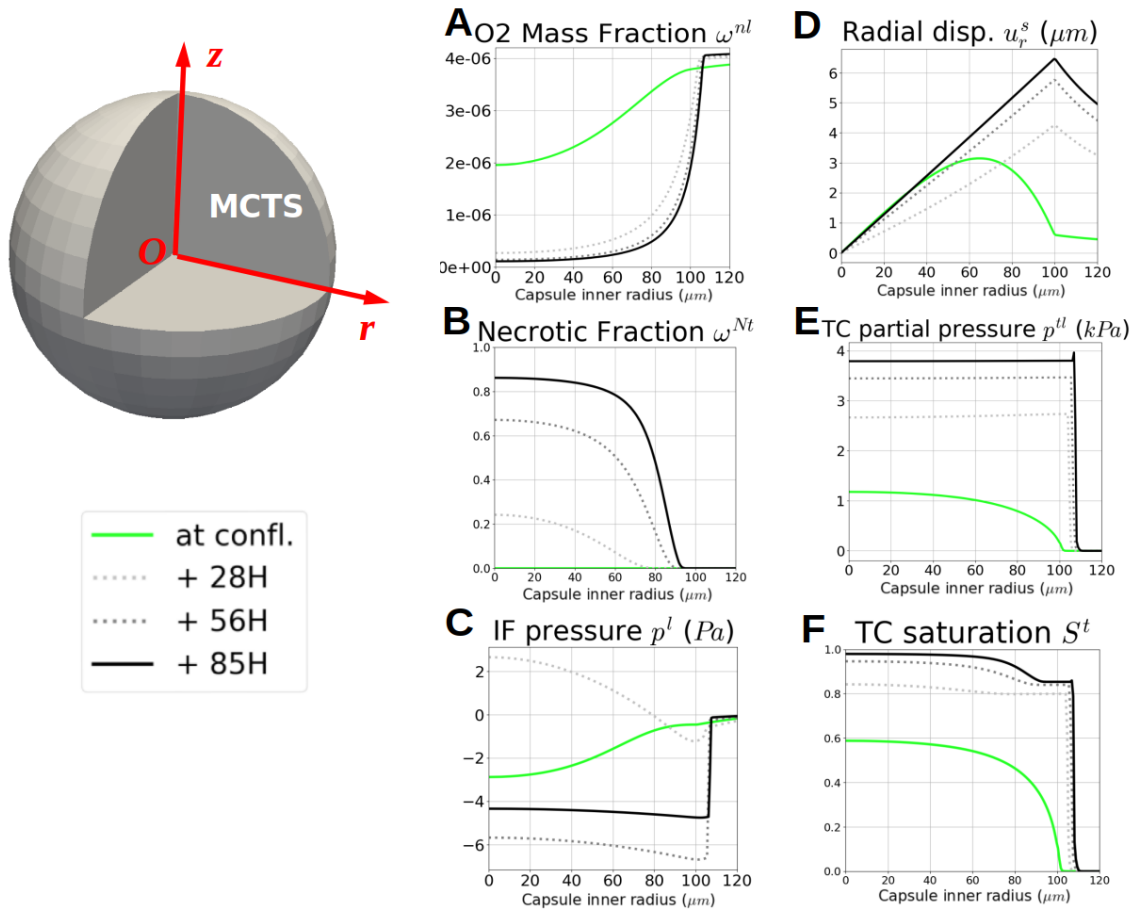


**Figure 5.** Quantities probed along the $r = z$ line at confluence, 85 hours after, and two intermediate times (28 and 56 hours): **A** oxygen, **B** necrotic fraction, **C** IF pressure, **D** ECM displacement, **E** TC pressure and **F** TC saturation. **A** and **B**: as mentioned in the experiments, 85 hours after confluence the viable space remaining for TC is a $20\,\mu$m thick rim. **C**: after confluence, IF is absorbed by growing TC, provoking a sucking phenomenon, as the cells activity decrease at the MCTS inner core, IF accumulates and its pressure becomes positive. As described in ***Alessandri et al.*** (***2013***), after 2 days of quick growth, the MTCS reaches a state of linear and slow evolution. **D** and **E**: the capsule displacement is driven by TC pressure with the same overall dynamic. **E**, **F** and **B**: relation between the saturation of TC and their necrotic fraction, the TC aggregate density increases with necrotic core.

bioRxiv preprint doi: https://doi.org/10.1101/2020.06.09.142927; this version posted October 10, 2020. The copyright holder for this preprint (which was not certified by peer review) is the author/funder, who has granted bioRxiv a license to display the preprint in perpetuity. It is made available under a CC-BY-NC-ND 4.0 International license.
Manuscript submitted to Cell

cells pressure $p^t$ does not determine directly the capsule deformation, which is more directly driven by the solid pressure, $p^s$ (see definition eq.21 in the Appendix A. The Multiphase System). The pressure $p^s$ is more representative of the average internal pressure obtained experimentally by inverse analysis (see Appendix C. Sensitivity analysis eq.39). At the confluence time, $p^s$ is importantly lower than the pressure in the tumor cell phase since at that time the MCTS consists also of $40\%$ of IF. After confluence the saturation of tumor cells increases progressively, so $p^s$, becomes closer to the pressure sustained by the cells.

In the presented physics-based approach, mass conservation is prescribed, so the growing MCTS, which increases in density and size, have to lead to a decreasing mass of interstitial fluid. This result, which cannot be measured experimentally, is shown in ***Figure 5*** where a sucking phenomenon due to IF absorption by growing TC can be observed. The ***Figure 5***C shows that after confluence the interstitial fluid pressure becomes positive during a while (see plot relative to 28h). Indeed, after confluence the initial gradient of IF pressure (green line in ***Figure 5***C) reverses since cells in the proliferative peripheral areas move toward the core so IF has to go in the opposite direction, as imposed physically by mass conservation. After 2 days of quick growth, experimentally and numerically, the MTCS reaches a state of linear and slow evolution and from that point onward, the IF flux will not qualitatively change.

To further analyze the reliability of the mathematical model we also exploit additional data of cell states inside MCTS presented in ***Alessandri et al.*** (***2013***). More specifically, we reproduced numerically a CT26-MCTS growing in free conditions and in a capsule having a radius of $50\mu$m. ***Figure 6***A and ***Figure 6***B present experimental cell densities (total, proliferative and necrotic) at $50\mu$m radius for the free MCTS and 26h after confluence for the confined MCTS. These experimental results are qualitatively compared with the numerical simulations (***Figure 6***C and ***Figure 6***D for the free and confined cases respectively). Both configurations show a reasonable agreement with the experimental results, knowing that none of these quantities have been used for the parameters identification, this is a supplementary argument for the adaptability of this physical based modelling.

## Discussion

We show in this paper the *in silico* reproduction of MCTS growth experiments in various physical conditions: free and encapsulated within alginate shells of different sizes and thicknesses. Thanks to a robust validation protocol, variance-based sensitivity analysis, distinct training and validation data sets, all these physical conditions have been successfully simulated by means of a bio-chemo-poromechanical mathematical model. It is important to notice that only one set of parameters, identified on a training data set (reported in ***Figure 1***C and ***Figure 1***D), has been used for all the numerical simulations performed.

In the frame of the parameter identification process a second order sensitivity analysis has revealed that the parameters of the model become almost independent under confinement (see ***Figure 2***D). Results of sensitivty analyses also demonstrate, that if the tumor is free to grow the only influential parameters are the proliferation and the oxygen consumption rates. Conversely, when the tumor growth is constrained by the presence of the alginate capsule the value of the critical pressure beyond which mechanical stresses impact its growth is the main driver.

Sensibility studies have guided us on the development of bio-physically relevant constitutive relationships enabling the formulation of a mathematical model which remains reliable even when the growth conditions of the MCTS are modified. This is an advancement with respect of other numerical studies based on poromechanics which are quite qualitative (*e.g.* ***Sciumè et al.*** (***2013***) and ***Santagiuliana et al.*** (***2019***)) or solely connected with a reference experimental setup (*e.g.* ***Mascheroni et al.*** (***2016***)).

The mathematical model is the digital twin MCTS-capsule system since it takes into account mechanistically its real multiphase nature; hence, the numerical results add new dimensions to the Cellular Capsule Technology. In particular, it is shown that the pressure estimated experimentally is illustrative of the evolution of the solid pressure, $p^s$, (in the sense of porous media mechanics,

bioRxiv preprint doi: https://doi.org/10.1101/2020.06.09.142927; this version posted October 10, 2020. The copyright holder for this preprint (which was not certified by peer review) is the author/funder, who has granted bioRxiv a license to display the preprint in perpetuity. It is made available under a CC-BY-NC-ND 4.0 International license.
Manuscript submitted to bioRxiv

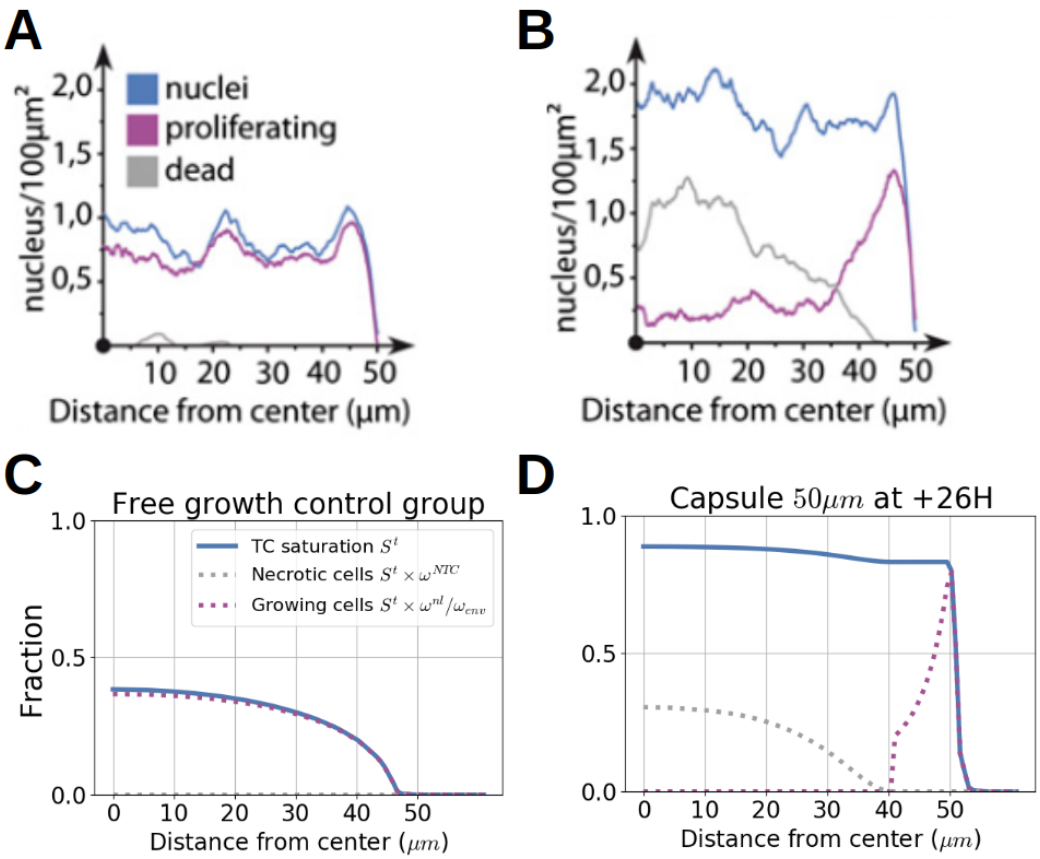


**Figure 6.** Quantification of proliferating and dead cells radial densities for free and confined CT26 spheroids: *in vitro-in silico* results. Experimental quantification of cell nuclei (blue), proliferating cells (purple),and dead cells (gray) along the radius for free, **A**, and confined, **B**, growth (from ***Alessandri et al.*** (***2013***)). Numerical results for 3 fractional quantities (TC Saturation $S^t$, blue, Necrotic saturation of TC $\omega^{Nt}S^t$, gray dotted, Growing TC fraction $\omega^{TC}_{\text{grow}}$ (see eq.31), purple dotted) vs distance from center in free, **C**, and encapsulated, **D**, configuration. TC saturation almost doubles between the two configurations, in encapsulation, necrotic fraction occupy almost half of the TC phase and only a thin rim of the MTCS is viable.

bioRxiv preprint doi: https://doi.org/10.1101/2020.06.09.142927; this version posted October 10, 2020. The copyright holder for this preprint (which was not certified by peer review) is the author/funder, who has granted bioRxiv a license to display the preprint in perpetuity. It is made available under a CC-BY-NC-ND 4.0 International license.


see eq.21 Appendix A. The Multiphase System) and not of the pressure sustained by the cells, $p^t$. The pressure $p^t$ is always higher than $p^s$ especially during the first phase after confluence (when the MTCS still contains an important volume fraction of IF). This fact is the direct consequence of the fact that each phase of the MCTS (*i.e.*, the ECM, the IF and the TC) has its own stress tensor and that the pressure obtained experimentally by inverse analysis is an average pressure. The multiphase approach also reveal other behaviours not measurable experimentally. We observe for instance that after confluence there is a suction of IF from the extra-capsular domain and that cells move from the proliferating rim towards the core of the MCTS where they become necrotic.

In 2020s mathematical modeling in oncology begins to enter a stage of maturity; today mathematical models of tumor growth tend to clinical applications and therefore must be really predictive and funded on measurable or at least quantifiable parameters having, as much as possible, a sound physical meaning. This motivated this paper which presents not only a mechanistic bio-chemo-poromechanical model but also a *modus procedendi* to achieve a suitable predicative potential and, with intercession of sensitivity analysis, to quantify relative relevance of mechanisms underlying tumor growth phenomenology.

## Acknowledgments

The authors acknowledge ENSAM *Réseau Santé* (health institutional network), fondation Arts et Métiers and University of Luxembourg that have financially supported the project as well as the funding of the University of Luxembourg, of the DRIVEN H2020 TWINNING Project 2020driven.uni.lu

## References

**Alessandri K**, Sarangi BR, Gurchenkov VV, Sinha B, Kießling TR, Fetler L, Rico F, Scheuring S, Lamaze C, Simon A, Geraldo S, Vignjević D, Doméjean H, Rolland L, Funfak A, Bibette J, Bremond N, Nassoy P. Cellular capsules as a tool for multicellular spheroid production and for investigating the mechanics of tumor progression in vitro. Proceedings of the National Academy of Sciences. 2013; 110(37):14843–14848. https://www.pnas.org/content/110/37/14843.

**Alnæs M**, Blechta J, Hake J, Johansson A, Kehlet B, Logg A, Richardson C, Ring J, Rognes M, Wells G. The FEniCS Project Version 1.5. Archive of Numerical Software. 2015; 3(100). http://journals.ub.uni-heidelberg.de/index.php/ans/article/view/20553.

**Benzekry S**, Lamont C, Beheshti A, Tracz A, Ebos JML, Hlatky L, Hahnfeldt P. Classical Mathematical Models for Description and Prediction of Experimental Tumor Growth. PLOS Computational Biology. 2014 08; 10(8):1–19. https://doi.org/10.1371/journal.pcbi.1003800, doi: 10.1371/journal.pcbi.1003800.

**Boffi D**, Brezzi F, Fortin M. Mixed Finite Element Methods and Applications. Springer; 2013.

**Brady R**, Enderling H. Mathematical Models of Cancer: When to Predict Novel Therapies, and When Not to. Bulletin of Mathematical Biology. 2019; doi: https://doi.org/10.1007/s11538-019-00640-x.

**Casciari JJ**, Sotirchos SV, Sutherland RM. Mathematical modelling of microenvironment and growth in EMT6/Ro multicellular tumour spheroids. Cell Proliferation. 1992; 25(1):1–22. https://onlinelibrary.wiley.com/doi/abs/10.1111/j.1365-2184.1992.tb01433.x, doi: 10.1111/j.1365-2184.1992.tb01433.x.

**Chignola R**, Schenetti A, Andrighetto G, Chiesa E, Foroni R, Sartoris S, Tridente G, Liberati D. Forecasting the growth of multicell tumour spheroids: implications for the dynamic growth of solid tumours. Cell Proliferation. 2000; 33(4):219–229. https://onlinelibrary.wiley.com/doi/abs/10.1046/j.1365-2184.2000.00174.x.

**Cukierman E**, Pankov R, Stevens DR, Yamada KM. Taking Cell-Matrix Adhesions to the Third Dimension. Science. 2001; 294(5547):1708–1712. https://science.sciencemag.org/content/294/5547/1708.

**Edgerton ME**, Chuang YL, Macklin P, Yang W, Bearer EL, Cristini V. A Novel, Patient-Specific Mathematical Pathology Approach for Assessment of Surgical Volume: Application to Ductal Carcinoma *in situ* of The Breast. Analytical Cellular Pathology. 2011; 34.

**Gray WG**, Miller CT. Introduction to the Thermodynamically Constrained Averaging Theory for Porous Medium Systems. Springer; 2014.

bioRxiv preprint doi: https://doi.org/10.1101/2020.06.09.142927; this version posted October 10, 2020. The copyright holder for this preprint (which was not certified by peer review) is the author/funder, who has granted bioRxiv a license to display the preprint in perpetuity. It is made available under a CC-BY-NC-ND 4.0 International license.
Manuscript submitted to Online

**Helmlinger G**, Netti PA, Lichtenbeld HC, Melder RJ, Jain RK. Solid stress inhibits the growth of multicellular tumor spheroids. Nature Biotechnology. 1997; 15(21):778–783.

**Jain RK**, Martin JD, Stylianopoulos T. The Role of Mechanical Forces in Tumor Growth and Therapy. Annual Review of Biomedical Engineering. 2014; 16(1):321–346. https://doi.org/10.1146/annurev-bioeng-071813-105259.

**Khan N**, Williams BB, Hou H, Li H, Swartz HM. Repetitive tissue pO2 measurements by electron paramagnetic resonance oximetry: current status and future potential for experimental and clinical studies. Antioxidants & redox signaling. 2007; 9(8):1169–1182.

**Koay EJ**, Truty MJ, Cristini V, Thomas RM, Chen R, Chatterjee D, Kang Y, Bhosale PR, Tamm EP, Crane CH, Javle M, Katz MH, Gottumukkala VN, Rozner MA, Shen H, Lee JE, Wang H, Chen Y, Plunkett W, Abbruzzese JL, et al. Transport properties of pancreatic cancer describe gemcitabine delivery and response. The Journal of clinical investigation. 2014; 124(4):1525–1536.

**Lorenzo G**, Hughes TJR, Dominguez-Frojan P, Reali A, Gomez H. Computer simulations suggest that prostate enlargement due to benign prostatic hyperplasia mechanically impedes prostate cancer growth. Proceedings of the National Academy of Sciences. 2019; 116(4):1152–1161. https://www.pnas.org/content/116/4/1152.

**Lowengrub JS**, Frieboes HB, Jin F, Chuang YL, Li X, Macklin P, Wise SM, Cristini V. Nonlinear modelling of cancer: bridging the gap between cells and tumours. Nonlinearity. 2010; 23(1).

**Mascheroni P**, Stigliano C, Carfagna M, Boso DP, Preziosi L, Decuzzi P, Schrefler BA. Predicting the growth of glioblastoma multiforme spheroids using a multiphase porous media model. Biomechanics and Modeling in Mechanobiology. 2016; 15(1):1215–1228.

**Ortiz-Prado E**, Dunn JF, Vasconez J, Castillo D, Viscor G, Warner F, Zucker SW. Partial pressure of oxygen in the human body: a general review. American journal of blood research. 2019; 9(1):1–14.

**Paszek MJ**, Zahir N, Johnson KR, Lakins JN, Rozenberg GI, Gefen A, Reinhart-King CA, Margulies SS, Dembo M, Boettiger D, Hammer DA, Weaver VM. Tensional homeostasis and the malignant phenotype. Cancer cell. 2005; 8:241–254.

**Santagiuliana R**, Milosevic M, Milicevic B, Sciumè G, Simic V, Ziemys A, Kojic M, Schrefler BA. Coupling tumor growth and bio distribution models. Biomedical microdevices. 2019; 21.

**Sciumè G**, Ferrari, Schrefler BA. Saturation–pressure relationships for two- and three-phase flow analogies for soft matter. Mechanics Research Communications. 2014d; 62:132–137.

**Sciumè G**, Gray WG, Hussain F, Ferrari M, Decuzzi P, Schrefler BA. Three phase flow dynamics in tumor growth. Computational Mechanics. 2014c; 53(3):465–484.

**Sciumè G**, Santagiuliana R, Ferrari M, Decuzzi P, Schrefler BA. A tumor growth model with deformable ECM. Physical biology. 2014a; 11(6).

**Sciumè G**, Shelton S, Gray WG, Miller CT, Hussain F, Ferrari M, Decuzzi P, Schrefler BA. A multiphase model for three-dimensional tumor growth. New Journal of Physics. 2013 jan; 15(1):015005. https://doi.org/10.1088/1367-2630/15/1/015005.

**Sciumè G**, Boso DP, Gray WG, Cobelli C, Schrefler BA. A two-phase model of plantar tissue: a step toward prediction of diabetic foot ulceration. International Journal for Numerical Methods in Biomedical Engineering. 2014b; 30(11):1153–1169. https://onlinelibrary.wiley.com/doi/abs/10.1002/cnm.2650.

**Stein E**, de Borst R, Hughes TJR. Encyclopedia of Computational Mechanics, Vol. 1. Wiley; 2017.

**Verruijt A**, Theory and Problems of Poroelasticity; 2013. https://geo.verruijt.net/.

## Appendix A. The Multiphase System

We give in this section all the details about governing equations and the constitutive relationships. According to the different phases, solid scaffold $s$, medium/interstitial fluid $l$ and tumor cells phase $t$, described in the main article, section Methods, which constitute the multiphase system, at each point in the domain, the following constraint must be respected

$$\varepsilon^s + \varepsilon^t + \varepsilon^l = 1, \tag{4}$$

bioRxiv preprint doi: https://doi.org/10.1101/2020.06.09.142927; this version posted October 10, 2020. The copyright holder for this preprint (which was not certified by peer review) is the author/funder, who has granted bioRxiv a license to display the preprint in perpetuity. It is made available under a CC-BY-NC-ND 4.0 International license.
Manuscript submitted to

where $\varepsilon^{\alpha}$ is the volume fraction of phase $\alpha$. Defining the porosity $\varepsilon$ as

$$\varepsilon = 1 - \varepsilon^{s}, \tag{5}$$

Equation 4 can also be expressed in terms of the saturation degree of the fluid phase, $S^{f} = \varepsilon^{f}/\varepsilon$ (with $f = t, l$)

$$S^{t} + S^{l} = 1. \tag{6}$$

## Mass conservation equations

We express the mass conservation equation for each phase. We use a material description for the motion of the solid phase and a spatial description for the fluid phases, whose reference space is that occupied by the solid scaffold. As the solid is deformable, this reference space is not fixed in time but evolves according to the displacement of the solid phase. For this reason we express mass conservation equations for each phase and species in their material form with respect to the solid scaffold velocity. Mass conservation equations of solid, cell and interstitial fluid phases read:

$$\frac{D^{s}}{Dt}(\rho^{s}\varepsilon^{s}) + \rho^{s}\varepsilon^{s}\nabla\cdot\mathbf{v}^{\bar{s}} = 0, \tag{7}$$

$$\frac{D^{s}}{Dt}\left(\rho^{t}\varepsilon S^{t}\right) + \nabla\cdot(\rho^{t}\varepsilon S^{t}\mathbf{v}^{\bar{t}s}) + \rho^{t}\varepsilon S^{t}\nabla\cdot\mathbf{v}^{\bar{s}} = \sum_{i\in l}\overset{il\to t}{M}, \tag{8}$$

$$\frac{D^{s}}{Dt}\left(\rho^{l}\varepsilon S^{l}\right) + \nabla\cdot(\rho^{l}\varepsilon S^{l}\mathbf{v}^{\bar{l}s}) + \rho^{l}\varepsilon S^{l}\nabla\cdot\mathbf{v}^{\bar{s}} = -\sum_{i\in l}\overset{il\to t}{M}, \tag{9}$$

where $\frac{D^{s}}{Dt}$ is the material time derivative with respect to the solid phase, $\rho^{\alpha}$ is the density of phase $\alpha$, $\mathbf{v}^{\bar{s}}$ is the velocity vector of the solid phase, $\sum_{i\in l}\overset{il\to t}{M}$ is the total mass exchange (water, oxygen and other nutrients) from the interstitial fluid to the tumor due to cell growth and metabolism, $\mathbf{v}^{\bar{t}s}$ is the relative velocity of cells, and $\mathbf{v}^{\bar{l}s}$ is relative velocity of the interstitial fluid.
The tumor cell phase is a mixture of living (LTC) and necrotic tumor cells (NTC), with mass fraction $\omega^{\bar{L}t}$ and $\omega^{\bar{N}t}$, respectively. The following constraint applies

$$\omega^{\bar{L}t} + \omega^{\bar{N}t} = 1. \tag{10}$$

Mass conservation equations for each fraction, assuming that there is no diffusion of both necrotic and living cells, read

$$\frac{D^{s}}{Dt}\left(\rho^{t}\omega^{\bar{L}t}\varepsilon S^{t}\right) + \nabla\cdot(\rho^{t}\omega^{\bar{L}t}\varepsilon S^{t}\mathbf{v}^{\bar{t}s}) + \rho^{t}\omega^{\bar{L}t}\varepsilon S^{t}\nabla\cdot\mathbf{v}^{\bar{s}} = \sum_{i\in l}\overset{il\to t}{M} - \varepsilon^{t}r^{Nt}, \tag{11}$$

$$\frac{D^{s}}{Dt}\left(\rho^{t}\omega^{\bar{N}t}\varepsilon S^{t}\right) + \nabla\cdot(\rho^{t}\omega^{\bar{N}t}\varepsilon S^{t}\mathbf{v}^{\bar{t}s}) + \rho^{t}\omega^{\bar{N}t}\varepsilon S^{t}\nabla\cdot\mathbf{v}^{\bar{s}} = \varepsilon^{t}r^{Nt}, \tag{12}$$

where $\varepsilon^{t}r^{Nt}$ is the death rate of tumor cells. Note that only one of Eqs 11-12 is independent: actually, one can be obtained subtracting the other from Eqn 8 and accounting for the constraint Eqn 10.
Oxygen is the only nutrient which we consider explicitly. Another mass balance equation is introduced which governs the advection-diffusion of oxygen, $n$, within the interstitial fluid

$$\frac{D^{s}}{Dt}\left(\rho^{l}\omega^{\bar{n}l}\varepsilon S^{l}\right) + \nabla\cdot(\rho^{l}\omega^{\bar{n}l}\varepsilon S^{l}\mathbf{v}^{\bar{l}s}) + \nabla\cdot(\rho^{l}\omega^{\bar{n}l}\varepsilon S^{l}\mathbf{u}^{\bar{n}l}) + \rho^{l}\omega^{\bar{n}l}\varepsilon S^{l}\nabla\cdot\mathbf{v}^{\bar{s}} = -\overset{nl\to t}{M}, \tag{13}$$

where $\mathbf{u}^{\bar{n}l}$ is the diffusive velocity of oxygen in the interstitial fluid and $\overset{nl\to t}{M}$ the oxygen consumed by tumor cells due to their metabolism and proliferation rate.

bioRxiv preprint doi: https://doi.org/10.1101/2020.06.09.142927; this version posted October 10, 2020. The copyright holder for this preprint (which was not certified by peer review) is the author/funder, who has granted bioRxiv a license to display the preprint in perpetuity. It is made available under a CC-BY-NC-ND 4.0 International license.


## Momentum conservation equations

We neglect here the effect of gravitational body forces as their contribution is negligible compared to that of other forces. Furthermore, as we assume quasi-static processes and small difference in density between cells and aqueous solutions, inertial forces and the force due to mass exchange can also be neglected. These assumptions simplify the general form of the linear momentum balance equation given in ***Gray and Miller*** (***2014***) which becomes

$$\nabla \cdot (\varepsilon^{\alpha}\mathbf{t}^{\bar{\bar{\alpha}}}) + \sum_{K\in\mathfrak{J}_{c\alpha}} \overset{K\to\alpha}{\mathbf{T}} = \mathbf{0} \quad (\alpha = s,t,l), \tag{14}$$

where $\mathbf{t}^{\bar{\bar{\alpha}}}$ is the stress tensor of phase $\alpha$, $\mathfrak{J}_{c\alpha}$ is the set phases connected to $\alpha$ and $\overset{K\to\alpha}{\mathbf{T}}$ is the interaction force between phase $\alpha$ and the adjacent phases. Summing eqn 14 over all phases gives the momentum equation of the whole multiphase system as

$$\nabla \cdot \mathbf{t}^{\bar{\bar{T}}} = \mathbf{0}, \tag{15}$$

where $\mathbf{t}^{\bar{\bar{T}}}$ is the total Cauchy stress tensor acting on the multiphase system.
Assuming that for relatively slow flow, the stress tensor for a fluid phase, $f$, can be properly approximated as

$$\mathbf{t}^{\bar{\bar{f}}} = -p^f\mathbf{1} \quad (f = t,l) \tag{16}$$

where $p^f$ is the averaged fluid pressure and $\mathbf{1}$ the unit tensor, Eqn. 14 which apply for a generic phase $\alpha$ (solid or fluid) can be expressed in an alternative form for fluid phases as ***Sciumè et al.*** (***2013***)

$$\varepsilon^f\nabla p^f + \mathbf{R}^f \cdot (\mathbf{v}^{\bar{f}} - \mathbf{v}^{\bar{s}}) = \mathbf{0} \quad (f = t,l) \tag{17}$$

where $\mathbf{R}^f$ is a symmetric second order resistance tensor accounting for interaction between the fluid phase and the solid phase, $s$. Eqn. 17 can be rewritten as

$$-\mathbf{K}^f \cdot \nabla p^f = \varepsilon^f(\mathbf{v}^{\bar{f}} - \mathbf{v}^{\bar{s}}) \quad (f = t,l), \tag{18}$$

where $\mathbf{K}^f = (\varepsilon^f)^2(\mathbf{R}^f)^{-1}$ is called the hydraulic conductivity. The hydraulic conductivity depends on the dynamic viscosity of the flowing fluid, $\mu^f$, on the intrinsic permeability of the porous scaffold, $k$, and on the fluid saturation degree, $S^f$, via a relative permeability function $k^f_{\text{rel}}(S^f) = (S^f)^A$ ($A$ depending on the fluid characteristics, see ***Sciumè et al.*** (***2014c***)). As customary in biphasic flow problems we set here $\mathbf{K}^f = k\frac{k^f_{\text{rel}}(S^f)}{\mu^f}\mathbf{1}$. Hence, the governing linear momentum conservation equations for tumor cells and interstitial fluid read

$$-k\frac{k^t_{\text{rel}}(S^t)}{\mu^t}\nabla p^t = \varepsilon^t(\mathbf{v}^{\bar{t}} - \mathbf{v}^{\bar{s}}), \tag{19}$$

$$-k\frac{k^l_{\text{rel}}(S^l)}{\mu^l}\nabla p^l = \varepsilon^l(\mathbf{v}^{\bar{l}} - \mathbf{v}^{\bar{s}}), \tag{20}$$

## Effective stress principle and closure relationships

We assume here that fluid phases are incompressible and the solid phase is almost incompressible. However, the overall multiphase system is not incompressible, because of the presence of porosity that evolves according with the scaffold deformation. As phases are incompressible, their densities $\rho^{\alpha}$ with $\alpha = s,t,l$ are constant. As the solid phase is quasi incompressible, the Biot's coefficient is set to unity. With these premises, the total Cauchy stress tensor appearing in eqn 15 is related to the Biot's effective stress as follows

$$\mathbf{t}^{\bar{\bar{E}}} = \mathbf{t}^{\bar{\bar{T}}} + p^s\mathbf{1}, \tag{21}$$

where $p^s = S^t p^t + S^l p^l$ is the so-called solid pressure, describing the interaction between the two fluids and the solid scaffold.

bioRxiv preprint doi: https://doi.org/10.1101/2020.06.09.142927; this version posted October 10, 2020. The copyright holder for this preprint (which was not certified by peer review) is the author/funder, who has granted bioRxiv a license to display the preprint in perpetuity. It is made available under a CC-BY-NC-ND 4.0 International license.


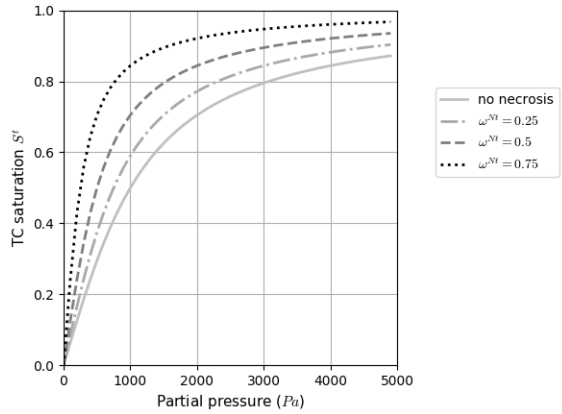


**Appendix 0 Figure 7.** Tumor cell phase saturation $S^t$, with the parameter $a$ fixed to 1kPa, evolving with the necrotic fraction of the phase $\omega^{\bar{N}t}$

The chosen closure relationship for the effective stress $\mathbf{t}^{\bar{\bar{E}}}$ is linear elastic:

$$\mathbf{t}^{\bar{\bar{E}}} = \bar{\bar{\bar{\bar{C}}}} : \epsilon(\mathbf{u}^{\bar{s}}), \tag{22}$$

with $\epsilon(u^s) = \frac{1}{2}(\nabla \mathbf{u}^{\bar{s}} + (\nabla \mathbf{u}^{\bar{s}})^T)$ and $\bar{\bar{\bar{\bar{C}}}}(\lambda, \mu)$ the fourth order elasticity tensor, reduced in Voigt notation: $\begin{pmatrix} \lambda+2\mu & \lambda & \lambda & 0 & 0 & 0 \\ \lambda & \lambda+2\mu & \lambda & 0 & 0 & 0 \\ \lambda & \lambda & \lambda+2\mu & 0 & 0 & 0 \\ 0 & 0 & 0 & \mu & 0 & 0 \\ 0 & 0 & 0 & 0 & \mu & 0 \\ 0 & 0 & 0 & 0 & 0 & \mu \end{pmatrix}$

with the Lamé constant $\lambda = \dfrac{E\nu}{(1+\nu)(1-2\nu)}$ and $\mu = \dfrac{E}{2(1+\nu)}$.
$E$ the Young modulus of the solid scaffold and $\nu$ its Poisson ratio.
The experimental measurement of cells density inside the capsule revealed a strong dependency to necrotic fraction $\omega^{\bar{N}t}$. Hence, the pressure-saturation closure relationship has been improved with respect to that proposed in ***Sciumè et al.*** (***2014a***), to be more physically relevant and adapted to confinement situation

$$S^t = \frac{2}{\pi} \arctan\left(\frac{p^{tl}}{(1-\omega^{\bar{N}t})a}\right), \tag{23}$$

with $p^{tl}$ pressure difference between tumor and interstitial fluid (i.e. $p^{tl} = p^t - p^l$). The saturation is directly linked to the partial pressure of the phase and a constant parameter $a$, which accounts for the effect of cell surface tension and of the refinement of the porous network (see ***Sciumè et al.*** (***2014d***) for the biophysical justification of the proposed equation). Its influence is offset by the necrotic fraction of tumor cells, $\omega^{\bar{N}t}$ (see Fig.***Figure 7***), which allows us to model necrotic areas of very high cell density according with experimental evidence.

## Tumor cells growth, metabolism and necrosis

The tumor cells growth, metabolism and necrosis are regulated by a variety of nutrient species and intracellular signalling. However, without losing generality, in the present model one single nutrient is considered: oxygen. The case of multiple species can be easily obtained as a straightforward extension of the current formulation. The Fick's law, adapted to porous medium, was adopted to model diffusive flow of oxygen eq.13:

$$\omega^{\bar{n}l}\mathbf{u}^{\bar{n}l} = -D^{nl}\nabla\omega^{nl} \tag{24}$$

bioRxiv preprint doi: https://doi.org/10.1101/2020.06.09.142927; this version posted October 10, 2020. The copyright holder for this preprint (which was not certified by peer review) is the author/funder, who has granted bioRxiv a license to display the preprint in perpetuity. It is made available under a CC-BY-NC-ND 4.0 International license.


where $D^{nl}$ the diffusion coefficient for oxygen in the interstitial fluid is defined by the constitutive equation from ***Sciumè et al.*** (***2014c***)

$$D^{nl} = D_0^{nl}(\varepsilon S^l)^{\delta}, \tag{25}$$

the exponent $\delta$ sets to $2$ (see ***Sciumè et al.*** (***2014a***), ***Mascheroni et al.*** (***2016***), ***Santagiuliana et al.*** (***2019***)).

Tumor cell growth is related to the exchange of nutrients between the IF and the living fraction of the tumor. The total mass exchange from IF to the tumor cell phase is defined as

$$\sum_{i\in l} \overset{il\to t}{M} = \gamma_g^t \mathcal{H}(\omega^{\bar{nl}})\left(1-\mathcal{H}_p(p^t)\right)\left(1-\omega^{\bar{N}t}\right)\varepsilon S^t, \tag{26}$$

Note that $\left(1-\omega^{\bar{N}t}\right)\varepsilon S^t$ is the living fraction of the tumor. $\gamma_g^t$ is the tumor growth rate parameter, cell-line dependent. $\mathcal{H}$ and $\mathcal{H}_p$ are regularized step functions varying between 0 and 1, with two threshold parameters $\sigma_1, \sigma_2$, that is to say $\mathcal{H} = \mathcal{H}(\sigma, \sigma_1, \sigma_2)$. When the variable $\sigma$ is greater than $\sigma_2$, $\mathcal{H}$ is equal to 1, it decreases progressively when the variable is between $\sigma_1$ and $\sigma_2$ and is equal to zero when the variable is lower that $\sigma_1$. $\mathcal{H}$ represent the growth dependency to oxygen:

$$\mathcal{H}(\omega^{\bar{nl}}, \omega_{\text{crit}}, \omega_{\text{env}}) = \begin{cases} 0 & \text{if} \quad \omega^{\bar{nl}} \le \omega_{\text{crit}} \\ \frac{1}{2} - \frac{1}{2}\cos\pi\frac{\omega^{\bar{nl}} - \omega_{\text{crit}}}{\omega_{\text{env}} - \omega_{\text{crit}}} & \text{if} \quad \omega_{\text{crit}} \le \omega^{\bar{nl}} \le \omega_{\text{env}} \\ 1 & \text{if} \quad \omega^{\bar{nl}} \ge \omega_{\text{env}} \end{cases} \tag{27}$$

$\omega_{\text{env}}$, the optimal oxygen mass fraction, is set to $4,2.10^{-6}$ which corresponds, according to Henry's law, to $90$mmHg, the usual oxygen mass fraction in arteries (see ***Ortiz-Prado et al.*** (***2019***)). $\omega_{\text{crit}}$, the hypoxia threshold, is cell-line dependent, for tumor cells, it has been set to a very low value: $10^{-6}$ ($\approx$ $20$mmHg, for common human tissue cells, hypoxic level is defined between $10$ and $20$mmHg ***Khan et al.*** (***2007***)) The function $\mathcal{H}(\omega^{\bar{nl}}, \omega_{\text{crit}}, \omega_{\text{env}})$ is plotted ***Figure 8***A.

Function $(1-\mathcal{H}_p)$ represents the dependency on pressure:

$$\mathcal{H}_p(p^t, p_1, p_{\text{crit}}) = \begin{cases} 0 & \text{if} \quad p^t \le p_1 \\ \sqrt{\frac{p^t - p_1}{p_{\text{crit}} - p_1}} & \text{if} \quad p_1 \le p^t \le p_{\text{crit}} \\ 1 & \text{if} \quad p^t \ge p_{\text{crit}} \end{cases} \tag{28}$$

An example of the function $\mathcal{H}_p(p^t, p_1, p_{\text{crit}})$ is plotted ***Figure 8***B, we have set $p_{\text{crit}}$ to 6kPa as initial guess (in ***Helmlinger et al.*** (***1997***), they found a inhibitory pressure at $10$kPa) and $p_1$, the pressure threshold when the inhibitory process starts, at $2$kPa.

As tumor grows, nutrients are taken up from the IF so that the sink term in eq.13 takes the following form:

$$\overset{nl\to t}{M} = \left[\gamma_g^{nl}\mathcal{H}(\omega^{\bar{nl}})\left(1-\mathcal{H}_p(p^t)\right) + \gamma_0^{nl}\tilde{\mathcal{H}}\right](1-\omega^{\bar{N}t})\varepsilon S^t, \tag{29}$$

Nutrient consumption from IF is due to two contributions: the growth of the tumor cells, as given by the first term within the square brackets in eq.29, the metabolism of the healthy cells, as presented in the second term. Thus, $\gamma_g^{nl}$ is related to the cell proliferation, as discussed above; whereas the coefficient $\gamma_0^{nl}$ relates to the cell metabolism. $\tilde{\mathcal{H}}$ is an adaptation of the previous step functions for the cell metabolism:

$$\tilde{\mathcal{H}}(\omega^{\bar{nl}}) = \begin{cases} 1 & \text{if} \quad \omega^{\bar{nl}} \ge \omega_{\text{crit}} \\ \frac{1}{2} - \frac{1}{2}\cos\pi\frac{\omega^{\bar{nl}}}{\omega_{\text{crit}}} & \text{else} \end{cases} \tag{30}$$

bioRxiv preprint doi: https://doi.org/10.1101/2020.06.09.142927; this version posted October 10, 2020. The copyright holder for this preprint (which was not certified by peer review) is the author/funder, who has granted bioRxiv a license to display the preprint in perpetuity. It is made available under a CC-BY-NC-ND 4.0 International license.


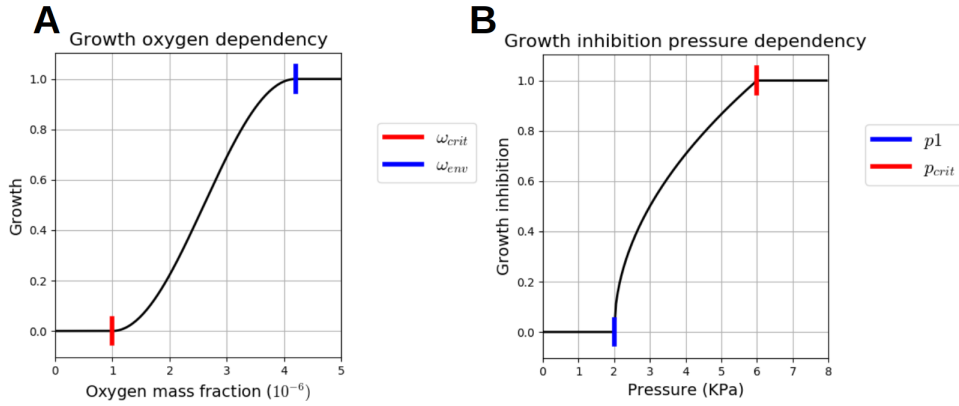


**Appendix 0 Figure 8.** Two mechano-biological laws. **A** $\mathcal{H}(\omega^{\bar{nl}}, \omega_{\text{env}}, \omega_{\text{crit}})$. The TC growth and nutrient consumption are dependent to the oxygen mass fraction $\omega^{\bar{nl}}$. If it is lower than $\omega_{\text{crit}}$, the TC growth is stopped and the nutrient consumption is reduced to the metabolism needs only. If it is greater or equal to $\omega_{\text{env}}$, the growth and the nutrient consumption are maximum. **B** $\mathcal{H}_p(p^t, p_{\text{crit}}, p_1)$. The TC growth and nutrient consumption are dependent to the TC pressure. If it is greater than $p_1$, the 2 processes begin to be strongly affected and if the TC pressure reaches $p_{\text{crit}}$, they are totally stopped.

The model does not discriminate between proliferating and quiescent cells, but the growth is subject to $\mathcal{H}(\omega^{\bar{nl}}, \omega_{\text{crit}}, \omega_{\text{env}})$. To make possible the comparison with the experimental proliferative cell quantities (see ***Figure 6***), the following relationship has been set:

$$\omega^{TC}_{\text{grow}} = \begin{cases} 0 \quad \text{if} \quad \omega^{\bar{nl}} \leq \omega_{\text{crit}} \\ S^t \dfrac{\omega^{\bar{nl}}}{\omega_{\text{env}}} \quad \text{else} \end{cases} \tag{31}$$

$\tilde{\mathcal{H}}$ is also used in the definition of hypoxic necrosis rate which reads

$$\varepsilon S^t r^{Nt} = \gamma^{Nt}(1 - \tilde{\mathcal{H}}(\omega^{\bar{nl}}))(1 - \omega^{\bar{N}t})\varepsilon S^t, \tag{32}$$

where $\gamma^{Nt} = 0.01$ is the necrotic growth rate. As the experimental data on necrosis were to sparse for this parameter identification (only a few stained cells imaging), we have kept its generic value.

## Appendix B. Computational framework

The model has been coded in Python and C++ in the open-source FEniCS framework ***Alnæs et al.*** (***2015***) with an incremental monolithic resolution of the mixed finite element (FE) formulation. The monolithic resolution allows us to reduce substantially the computational time compared with staggered resolution methods usually adopted (*e.g.* see ***Sciumè et al.*** (***2014b***). Whereas spherical symmetry is assumed in experimental results, we have chosen cylindrical symmetry to preserve the generality and the adaptability of the FE mesh and formulation. Even if the computational time is more important, it remains reasonable: 3 hours in a single core of an average laptop ; 1D spherical formulation would have forced us to quit classical FE formulation or to design, for each case, a specific finite difference formulation.

The simulations have been run with composite Taylor-Hood element $P_3(\mathbb{R}^2)$, $[P_2(\mathbb{R})]^3$ (one vectorial and three scalar unknowns), a mesh cell size of $dh = 5\mu$m and an implicit Euler scheme with $dt = 1200$ s. An updated lagrangian approach has been adopted to account for geometrical nonlinearities, the incremental resolution allows us to update primary variables as follows:

$$\mathbf{X}_{n+1} = \mathbf{X}_n + \delta\mathbf{X} \tag{33}$$

bioRxiv preprint doi: https://doi.org/10.1101/2020.06.09.142927; this version posted October 10, 2020. The copyright holder for this preprint (which was not certified by peer review) is the author/funder, who has granted bioRxiv a license to display the preprint in perpetuity. It is made available under a CC-BY-NC-ND 4.0 International license.


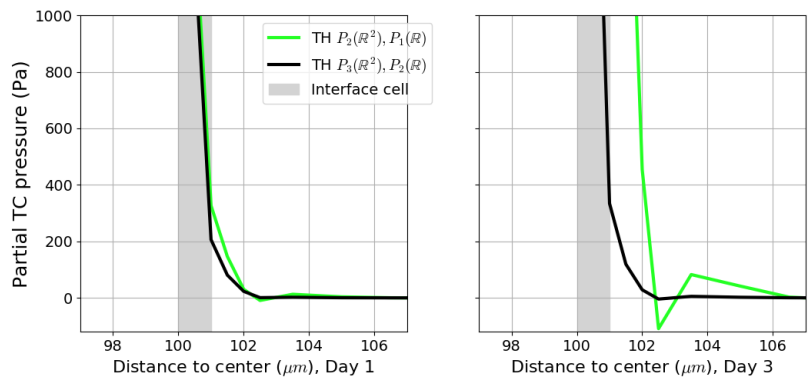


**Appendix 0 Figure 9.** Choice of the element (composite Taylor-Hood $P_2(\mathbb{R}^2), [P_1(\mathbb{R})]^3$, green ; composite Taylor-Hood $P_3(\mathbb{R}^2), [P_2(\mathbb{R})]^3$, brown). The linear approximation $P_1(\mathbb{R})$ of the partial tumor cells pressure at the capsule interface (Interface element shared, black) is poor (Left, Day 1) and provoke numerical infiltration of tumor cells into the alginate capsule (Right, Day 3)

---

with $\delta\mathbf{X}$ the vector of unknowns

$$\delta\mathbf{X} = \begin{pmatrix} \delta u_r^s \\ \delta u_z^s \\ \delta p^l \\ \delta p^{tl} \\ \delta \omega^{\bar{n}l} \end{pmatrix}$$

After each time step, the space $\mathcal{X}^s \in \mathbb{R}^2$ is updated:

$$\mathcal{X}_{n+1}^s = \mathcal{X}_n^s + \delta\mathbf{u}^s$$

All the codes used in this article, analytical verification, free growth and confined growth, are available on Github, at https://github.com/StephaneUrcun/MCTS_mechanics

## Choice of the element

For all mixed FE problem with vectorial and scalar coupled unknowns, the chosen finite element should verify the inf-sup condition, that is to say, should preserve the coercivity of the bilinear form (see ***Boffi et al.*** (***2013***) p.223-230). A simple choice is the Taylor-Hood element, with a Lagrange element of order $k \geq 1$ for the scalar unknowns and order $k+1$ for the vectorial one. However, modelling an encapsulated tumor growth implies a very sharp gradient at the capsule inner radius for the partial pressure of the tumor cells phase $p^{tl}$. The linear approximation of the Lagrange element of order 1 could not describe it, except at the cost of an extremely refined mesh at the interface, and the error could provoke *numerical infiltration* of tumor cells in the alginate capsule (see Fig.***Figure 9***). To avoid this phenomenon, the composite Taylor-Hood element has been set to a higher order, precisely the mixed FE formulation in FEniCS uses the composite Taylor-Hood element $P_3(\mathbb{R}^2), [P_2(\mathbb{R})]^3$. The demonstration of Lax-Milgram theorem for this type of mixed problem could be found in the *Encyclopedia of Computational Mechanics*, Vol.1, p.149-202 ***Stein et al.*** (***2017***).

## Choice of the mesh cell size

The mixed FE problem has been computed on 5 different meshes, with uniform cell sizes $dh = 50, 20, 10, 5$ and $2.5\mu$m. To measure the FE solution degradation the primary variable $\omega^{\bar{n}l}$, the oxygen mass fraction, has been monitored at the spheroid center during 4 days (see Fig ***Figure 10***) . The thinner mesh of cell size $dh = 2.5\,\mu$m has been used as reference for the RMSE. Despite an important increase of the computation time, the mesh cell size of $dh = 5\,\mu$m has been chosen to restrict the relative degradation of the FE solution to $RMSE = 0.01$ (see Table 2).

bioRxiv preprint doi: https://doi.org/10.1101/2020.06.09.142927; this version posted October 10, 2020. The copyright holder for this preprint (which was not certified by peer review) is the author/funder, who has granted bioRxiv a license to display the preprint in perpetuity. It is made available under a CC-BY-NC-ND 4.0 International license.


**Appendix 0 Table 2.** Relative degradation of the solution due to mesh cell size. Measured by root mean square, the reference being the thinner mesh with a mesh cell size of $dh = 2.5\,\mu$m.

| | $dh = 50\,\mu$m | $dh = 20\,\mu$m | $dh = 10\,\mu$m | $dh = 5\,\mu$m |
|---|---|---|---|---|
| $RMSE(dh, 2.5\,\mu\text{m}, 400/dh)$ | 0.182 | 0.032 | 0.019 | 0.010 |

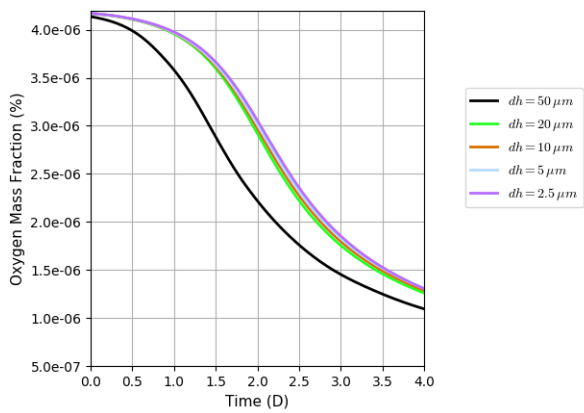


**Appendix 0 Figure 10.** Sensibility of the solution related to mesh refinement. The oxygen mass fraction, $\omega^{\bar{nl}}$, at the center of the spheroid has been monitored during six days for five different mesh cell sizes. ($dh = 50\,\mu$m, black ; $dh = 20\,\mu$m, green ; $dh = 10\,\mu$m, brown; $dh = 5\,\mu$m, light blue ; $dh = 2.5\,\mu$m, purple)

## Verification of the FE formulation with an analytical solution

If this system is considered with a single phase flow into a porous medium under a constant load with the right boundary conditions, one obtains the problem as known as Terzaghi's consolidation, which has an analytical solution ***Verruijt*** (***2013***). The system, under a constant load $\mathbf{T}$, is reduced to two primary variables the displacement of the solid scaffold $\mathbf{u}^s$ and the pressure of the single phase fluid $p^l$:

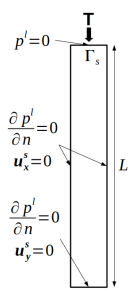


$$\begin{cases} \nabla.\mathbf{v}^s - \nabla.\left[\dfrac{k}{\mu}\nabla p^l\right] = 0 \text{ on } \Omega \\ \nabla.\bar{\bar{t}}_t = 0 \text{ on } \Omega \\ \nabla.\bar{\bar{t}}_t = -\mathbf{T} \text{ on } \Gamma_s \end{cases} \quad \text{with } \mathbf{T} = \begin{pmatrix} 0 \\ p_0 \end{pmatrix} \tag{34}$$

The fluid is free to escape only at the loaded boundary, this boundary condition is known as drying condition. The analytical solution of this problem is:

$$p^l(y,t) = p_0 \frac{4}{\pi} \sum_{k=1}^{\infty} \frac{(-1)^{k-1}}{2k-1} \cos\left((2k-1)\frac{\pi}{2}\frac{y}{L}\right) \exp\left((2k-1)^2 \frac{\pi^2}{4}\bar{t}\right) \tag{35}$$

With the characteristic time of the consolidation $\bar{t}$, equal to $\frac{c_v t}{L^2}$, $L$ sets to $100\,\mu$m and $c_v$, the consolidation coefficient:

$$c_v = \frac{k}{\mu^l}(\lambda + 2\mu)$$

where $\lambda$ and $\mu$ are Lamé constants of the solid scaffold, $k$ is its intrinsic permeability and $\mu^l$ the fluid dynamic viscosity. The addition of the RMSE of the 4 samples at $\bar{t} = 0.01, 0.1, 0.5, 1$ (see Fig.***Figure 11***) with the analytical solution as reference gives $\sum RMSE = 0.0028$. The surface error for different cell sizes $dh$ and time steps $dt$ is in Fig.***Figure 11***(right).

bioRxiv preprint doi: https://doi.org/10.1101/2020.06.09.142927; this version posted October 10, 2020. The copyright holder for this preprint (which was not certified by peer review) is the author/funder, who has granted bioRxiv a license to display the preprint in perpetuity. It is made available under a CC-BY-NC-ND 4.0 International license.
Manuscript submitted to *Cell*

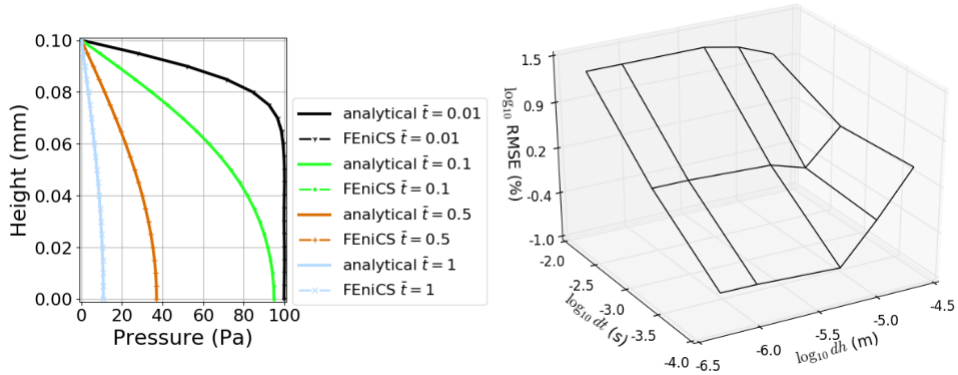


**Appendix 0 Figure 11.** Left: qualitative comparison between analytical solution of Terzaghi's problem and FEniCS computation. (4 comparisons at characteristic time of consolidation $\bar{t} = 0.01, 0.1, 0.5, 1$). Right: quantitative comparison: error surface between Terzaghi's analytical solution and FEniCS computation. (x axis: $\log_{10}$ of cell size $dh$ ; y axis: $\log_{10}$ of $dt$ ; z axis: $\log_{10}$ of RMSE). The minimum RMSE= $0.0028$ is reached at $dh = 5\mu$m, $dt = 1e^{-4}$

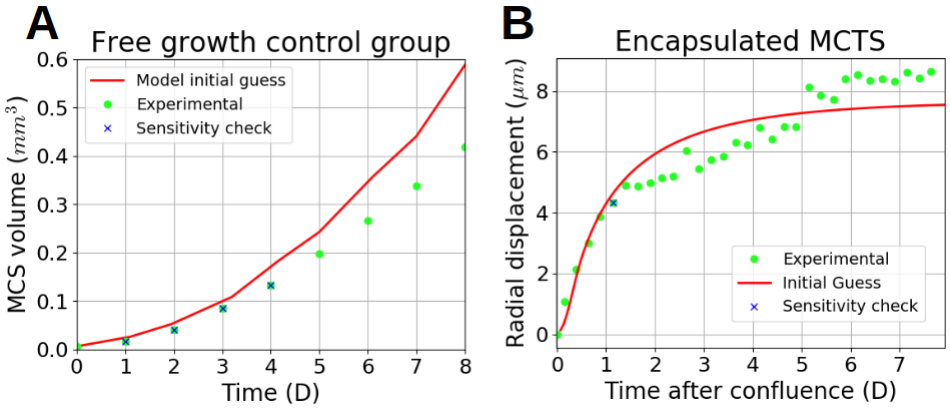


**Appendix 0 Figure 12.** Results with the 7 parameters at their initial values: $\gamma_g^t = 4.10^{-2}$, $\gamma_0^{nl} = 6.10^{-4}$, $a = 800$, $p_1 = 1800$, $p_{\text{crit}} = 4000$ (see Table 1). Experimental, green dot ; Model, red ; Sensitivity evaluation, blue x. Left: free growth ; Right: encapsulated growth

---

## Appendix C. Sensitivity analysis

For the sensitivity analysis, the experimental input data were:

- for the free MCTS, the volume monitored over a time span from day 1 to day 4. These data are denoted $Y_{\text{free}}^{\text{exp}}$
- for the encapsulated MCTS the capsule strain one day after confluence and the corresponding analytical pressure (i.e. incompressible elastic membrane). We chose the capsule of inner radius = $100\mu$m and thickness = $34\mu$m, presented as the reference case in ***Alessandri et al.*** (***2013***). These data are denoted $Y_{\text{conf}}^{\text{exp}}$.

We performed a variance-based sensitivity study of the FE solution on the parameters, both on the free and encapsulated MCTS, as follows:

- A first order analysis, the 7 parameters are disturbed one at a time respectively to a 8 points grid.
- Interaction analysis, the 21 parameters tuples are evaluated at the 2 extreme points of the grid.

All the results were interpreted with a polynomial model in order to quantify their weights in the FE solution variance, referred to as Sobol indices.

bioRxiv preprint doi: https://doi.org/10.1101/2020.06.09.142927; this version posted October 10, 2020. The copyright holder for this preprint (which was not certified by peer review) is the author/funder, who has granted bioRxiv a license to display the preprint in perpetuity. It is made available under a CC-BY-NC-ND 4.0 International license.


## Cost functions

In order to build a the cost function for the multiphase system with the sparse data available, a simulation noted $Y_{\text{goal}}$ has been run freely until it reaches the experimental volume corresponding to $Y_{\text{free}}^{\text{exp}}$, the experimental data of days 1,2,3 and 4. At the corresponding iterations, the numerical quantities have been stored. At day $i$, the tumor volume is equal to:

$$V_{\text{goal}_i} = \int_{\Omega} \varepsilon_i S_i^t \, dx$$

where $\Omega$ is the whole computation domain, as $S^t = 0$ outside of the tumor zone.
A second simulation with the same parameters has been run for 4 days and its volume has been compared to $Y_{\text{goal}}$ at the time steps corresponding to 1, 2, 3 and 4 days, noted $D_i \, (i = 1, 2, 3, 4)$. One can write this cost function explicitly:

$$J_{\text{free}}(X, \Phi) = \sum_{i=1}^{4} \int_{\Omega} \left[ \varepsilon(D_i) S^t(D_i) - \varepsilon_i S_i^t \right]^2 \, dx \tag{36}$$

For the encapsulated configuration, the cost function $J_{conf}(X, \Phi)|_T$ has the classical form:

$$J_{\text{conf}}(X, \Phi)|_{T_i} = \int_{\partial_{\text{Caps}}} < F(X, \Phi, T) - Y_{\text{conf}}^{\text{exp}}(T) > \, ds$$

Where the observable $Y_{\text{conf}}^{\text{exp}}$ has two components, $u(R_{\text{in}})$ the experimental measurement of the capsule inner radius at time $T_i$ after confluence ($\partial_{\text{Caps}}$ corresponding to the interface between the MCTS and the alginate capsule), and $P_{\text{conf}}$ the analytical pressure on capsule given in ***Alessandri et al.*** (***2013***), calculated using the formalism of thick-walled internally pressurized spherical vessels as follows: assuming that the alginate gel is isotropic and incompressible the radial displacement of the inner wall, $u(R_{\text{in}})$, reads

$$u(R_{\text{in}}) = \frac{3}{4} \frac{P_{\text{conf}}}{E} \frac{R_{\text{in}}}{1 - (R_{\text{in}}/R_{\text{out}})^3}. \tag{37}$$

where $P_{\text{conf}}$ is the internal pressure, $E$ is the Young's modulus, and $R_{\text{in}}$ and $R_{\text{out}}$ are the inner and outer radii of the capsule, respectively. Alginate incompressibility also implies volume conservation of the shell. This gives the following constraint equation

$$R_{\text{out}}^3(t) - R_{\text{in}}^3(t) = R_{\text{out}}^3(0) - R_{\text{in}}^3(0) = \delta(R_0^3) \tag{38}$$

Using this equation, the two time variables $R_{\text{in}}(t)$ and $R_{\text{out}}(t)$ can be separated and pressure, $P_{\text{conf}}(t)$, written as a function of $R_{\text{in}}(t)$ only

$$P_{\text{conf}}(t) = \frac{4}{3} E \left[ 1 - \frac{1}{1 + \delta(R_0^3)/R_{\text{in}}^3(t)} \right] \frac{u(R_{\text{in}}(t))}{R_{\text{in}}(t)} \tag{39}$$

The numerical approximation $F(X, \Phi, T)$ has the two corresponding components $(\mathbf{u}^s, p^s)$ in $\partial_{\text{Capsule}}$. We compared the FE solution with the experimental data 1 day after confluence. One can write this cost function explicitly[2]:

$$J_{\text{conf}}(X, \Phi)|_{\text{day 1}} = \int_{\partial_{\text{Caps}}} < \mathbf{u}(R_{\text{in}}) - \mathbf{u}^s > \, ds + \int_{\partial_{\text{Caps}}} (P_{\text{conf}} - p^s)^2 \, ds \tag{40}$$

Two simulations were run with the 7 parameters at their generic value (see ***Figure 12***). We denoted the respective cost functions $J0_{\text{free}}$ and $J0_{\text{conf}}$.

[2]For the cost function evaluation, $u(R_{\text{in}})$ a scalar experimental quantity, has been converted in vectorial quantity $\mathbf{u}(R_{\text{in}})$ with a constant norm on $\partial_{\text{Caps}}$ equal to $u(R_{\text{in}})$

bioRxiv preprint doi: https://doi.org/10.1101/2020.06.09.142927; this version posted October 10, 2020. The copyright holder for this preprint (which was not certified by peer review) is the author/funder, who has granted bioRxiv a license to display the preprint in perpetuity. It is made available under a CC-BY-NC-ND 4.0 International license.
Manuscript submitted to Cell

**Appendix 0 Table 3.** Sobol indices of the first order sensitivity analysis of the free growth configuration

| Parameter | $\theta$ | $S_i(\%)$ |
|---|---|---|
| $a$ | 0.2554 | 6.25 |
| $\mu_t$ | −0.1998 | 3.82 |
| $\gamma_g^t$ | 0.9205 | 81.17 |
| $\gamma_g^{nl}$ | −0.1161 | 1.29 |
| $\gamma_0^{nl}$ | −0.2790 | 7.45 |
| $p_1$ | 0 | 0 |
| $p_{\text{crit}}$ | 0 | 0 |

**Appendix 0 Table 4.** Sobol indices of the first order sensitivity analysis of the encapsulated growth configuration

| Parameter | $\theta$ | $S_i(\%)$ |
|---|---|---|
| $a$ | 0,0550 | 13.43 |
| $\mu_t$ | −0,0006 | 0.001 |
| $\gamma_g^t$ | 0,0371 | 6.11 |
| $\gamma_g^{nl}$ | −0,0056 | 0.14 |
| $\gamma_0^{nl}$ | −0,0271 | 3.27 |
| $p_1$ | 0,0279 | 3.45 |
| $p_{\text{crit}}$ | 0,1288 | 73.57 |

## First order analysis

Each parameter is disturbed one at a time respectively to this grid $[-10, -5, -2, -1, +1, +2, +5, +10]\%$, giving the corresponding $\tilde{J}_{\text{free}}$ and $\tilde{J}_{\text{conf}}$. The relative variations of the cost functions were calculated as follows:

$$\text{Var}_{\text{free}} = \frac{\tilde{J}_{\text{free}} - J0_{\text{free}}}{J0_{\text{free}}} \quad \text{and} \quad \text{Var}_{\text{conf}} = \frac{\tilde{J}_{\text{conf}} - J0_{\text{conf}}}{J0_{\text{conf}}} \tag{41}$$

In order to quantify the impact of each parameter, the following linear model was set:

$$\text{Var} = 1 + \sum_i \theta_i \alpha_i \tag{42}$$

where $\alpha_i$ is an auxiliary parameter $\in [-1, +1]$ representing the perturbations of the $i^{th}$ parameter along the grid and $\theta_i$ the slope of the variation.

In a first order analysis, the influence of the $i^{th}$ parameter is given by the Sobol indices:

$$S_i = \frac{\theta_i^2}{\sum_i \theta_i^2} \tag{43}$$

The results for the free and encapsulated configurations are reported in Tables 3 and 4.

## Interaction analysis

As the independence of physical phenomenons involved in both configuration is one our major modeling assessment, the interaction between parameters has also been studied. The 21 tuples have been evaluated at the 2 extreme values of the grid for each configuration. The corresponding polynomial model becomes:

$$\text{Var} = 1 + \sum_i \theta_i \alpha_i + \sum_{ij, i>j} \theta_{ij} \alpha_i \alpha_j \tag{44}$$

with the respective Sobol indices:

$$S_i = \frac{\theta_i^2}{\sum_i \theta_i^2 + \sum_{ij,i>j} \theta_{ij}^2} \quad \text{and} \quad S_{ij} = \frac{\theta_{ij}^2}{\sum_i \theta_i^2 + \sum_{ij,i>j} \theta_{ij}^2} \tag{45}$$

bioRxiv preprint doi: https://doi.org/10.1101/2020.06.09.142927; this version posted October 10, 2020. The copyright holder for this preprint (which was not certified by peer review) is the author/funder, who has granted bioRxiv a license to display the preprint in perpetuity. It is made available under a CC-BY-NC-ND 4.0 International license.


**Appendix 0 Table 5.** Sobol indices of the interaction sensitivity analysis of the free growth configuration

| Parameter | $S_i(\%)$ |
|---|---|
| $a$ | 5.11 |
| $\mu_t$ | 3.13 |
| $\gamma_g^t$ | 66.42 |
| $\gamma_g^{nl}$ | 1.05 |
| $\gamma_0^{nl}$ | 6.10 |
| $p_1$ | 0 |
| $p_{\text{crit}}$ | 0 |
| **Parameter tuples** | $S_{ij}(\%)$ |
| $(a,\ \mu_t)$ | 0.06 |
| $(a,\ \gamma_g^t)$ | 14.52 |
| $(a,\ \gamma_g^{nl})$ | 0.02 |
| $(a,\ \gamma_0^{nl})$ | $1.10^{-4}$ |
| $(\mu_t,\ \gamma_g^t)$ | 1.32 |
| $(\mu_t,\ \gamma_g^{nl})$ | 0.06 |
| $(\mu_t,\ \gamma_0^{nl})$ | 0.38 |
| $(\gamma_g^t,\ \gamma_g^{nl})$ | 1.20 |
| $(\gamma_g^t,\ \gamma_0^{nl})$ | 0.21 |
| $(\gamma_g^{nl},\ \gamma_0^{nl})$ | 0.37 |

The results for the free and encapsulated configurations are reported in Tables 5 and 6.

bioRxiv preprint doi: https://doi.org/10.1101/2020.06.09.142927; this version posted October 10, 2020. The copyright holder for this preprint (which was not certified by peer review) is the author/funder, who has granted bioRxiv a license to display the preprint in perpetuity. It is made available under a CC-BY-NC-ND 4.0 International license.
Manuscript submitted online

**Appendix 0 Table 6.** Sobol indices of the interaction sensitivity analysis of the encapsulated growth configuration

| Parameter | $S_i(\%)$ |
|---|---|
| $a$ | 12.96 |
| $\mu_t$ | 0.001 |
| $\gamma_g^t$ | 5.89 |
| $\gamma_g^{nl}$ | 0.13 |
| $\gamma_0^{nl}$ | 3.15 |
| $p_1$ | 3.33 |
| $p_{\text{crit}}$ | 70.94 |
| **Parameter tuples** | $S_{ij}(\%)$ |
| $(a,\ \mu_t)$ | 0.01 |
| $(a,\ \gamma_g^t)$ | 0.003 |
| $(a,\ \gamma_g^{nl})$ | 0.01 |
| $(a,\ \gamma_0^{nl})$ | 0.02 |
| $(a,\ p_1)$ | 0.009 |
| $(a,\ p_{\text{crit}})$ | 0.02 |
| $(\mu_t,\ \gamma_g^t)$ | 0.02 |
| $(\mu_t,\ \gamma_g^{nl})$ | $5.10^{-6}$ |
| $(\mu_t,\ \gamma_0^{nl})$ | 0.007 |
| $(\mu_t,\ p_1)$ | 0.003 |
| $(\mu_t,\ p_{\text{crit}})$ | 0.7 |
| $(\gamma_g^t,\ \gamma_g^{nl})$ | 0.02 |
| $(\gamma_g^t,\ \gamma_0^{nl})$ | 0.01 |
| $(\gamma_g^t,\ p_1)$ | $5.10^{-4}$ |
| $(\gamma_g^t,\ p_{\text{crit}})$ | 0.08 |
| $(\gamma_g^{nl},\ \gamma_0^{nl})$ | 0.01 |
| $(\gamma_g^{nl},\ p_1)$ | 0.002 |
| $(\gamma_g^{nl},\ p_{\text{crit}})$ | 0.87 |
| $(\gamma_0^{nl},\ p_1)$ | 0.01 |
| $(\gamma_0^{nl},\ p_{\text{crit}})$ | 1.30 |
| $(p_1,\ p_{\text{crit}})$ | 0.42 |